Article

Cell Reports

Aurora Kinase B Regulates Telomerase Activity via a Centromeric RNA in Stem Cells

Graphical Abstract

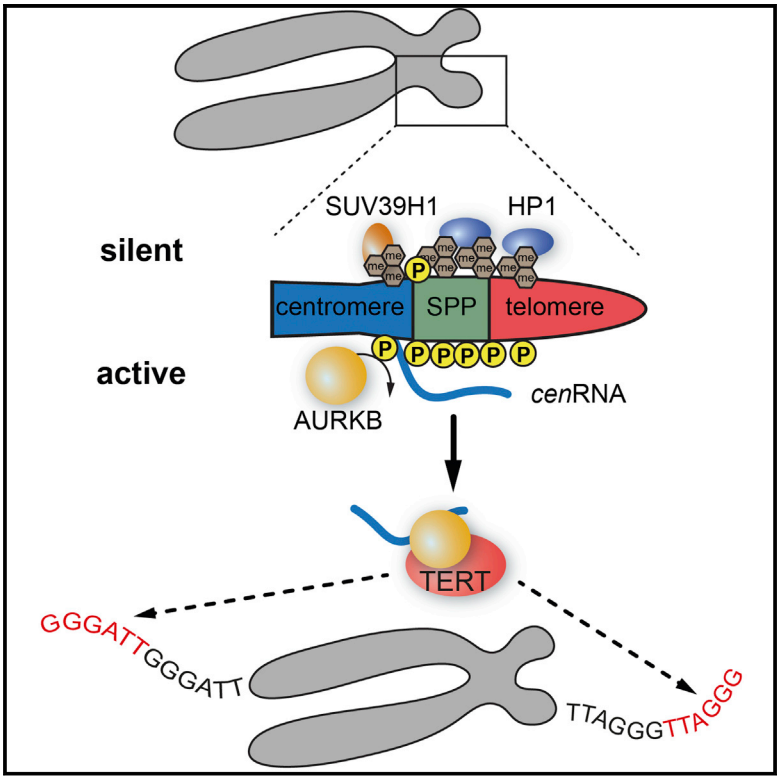

Authors

Jan-Philipp Mallm, Karsten Rippe

Correspondence

j.mallm@dkfz.de (J.-P.M.),
karsten.rippe@dkfz.de (K.R.)

In Brief

Mallm and Rippe find that AURKB kinase and centromeric RNA regulate telomerase activity. AURKB phosphorylates serine 10 of histone H3 at chromosome p-arms during S phase in embryonic stem cells to induce centromere repeat transcription. Together, AURKB and centromere transcripts activate telomerase and ensure telomere maintenance.

Highlights

- Embryonic stem cells have histone H3 serine 10 phosphorylation foci during S phase
- H3S10p foci are located at chromosome p-arms and are set by Aurora kinase B
- H3S10p opens up chromatin and induces transcription of centromere repeats
- Both AURKB and centromeric transcripts are needed for full activity of telomerase

Accession Numbers

GSE67133

Mallm & Rippe, 2015, Cell Reports *11*, 1667–1678
June 16, 2015
http://dx.doi.org/10.1016/j.celrep.2015.05.015

Cell Reports
Article

Aurora Kinase B Regulates Telomerase Activity via a Centromeric RNA in Stem Cells

Jan-Philipp Mallm[1,2,*] and Karsten Rippe[1,2,*]
[1]Research Group Genome Organization and Function, Deutsches Krebsforschungszentrum (DKFZ), Im Neuenheimer Feld 280, 69120 Heidelberg, Germany
[2]Bioquant Center, Im Neuenheimer Feld 267, 69120 Heidelberg, Germany
*Correspondence: j.mallm@dkfz.de (J.-P.M.), karsten.rippe@dkfz.de (K.R.)
http://dx.doi.org/10.1016/j.celrep.2015.05.015

SUMMARY

Non-coding RNAs can modulate histone modifications that, at the same time, affect transcript expression levels. Here, we dissect such a network in mouse embryonic stem cells (ESCs). It regulates the activity of the reverse transcriptase telomerase, which synthesizes telomeric repeats at the chromosome ends. We find that histone H3 serine 10 phosphorylation set by Aurora kinase B (AURKB) in ESCs during the S phase of the cell cycle at centromeric and (sub)telomeric loci promotes the expression of non-coding minor satellite RNA (*cen*RNA). Inhibition of AURKB induces silencing of *cen*RNA transcription and establishment of a repressive chromatin state with histone H3 lysine 9 trimethylation and heterochromatin protein 1 accumulation. This process results in a continuous shortening of telomeres. We further show that AURKB interacts with both telomerase and *cen*RNA and activates telomerase in *trans*. Thus, in mouse ESCs, telomere maintenance is regulated via expression of *cen*RNA in a cell-cycle-dependent manner.

INTRODUCTION

Phosphorylation of serine 10 of histone H3 (H3S10p) by Aurora kinase B (AURKB) is a well-established chromatin modification of mitotic chromosomes (Adams et al., 2001; Honda et al., 2003). During mitosis, H3S10 phosphorylation acts in concert with H3K14 acetylation (H3K14ac) and induces the dissociation of heterochromatin protein 1 (HP1) from chromatin (Fischle et al., 2005; Mateescu et al., 2004). The latter protein interacts with the SUV39H1 and SUV39H2 histone methylases (referred to here as SUV39H) that catalyze the di- and trimethylation of histone H3 at lysine 9 (H3K9me2/3) in pericentric heterochromatin (Aagaard et al., 1999; Müller-Ott et al., 2014; Yamamoto and Sonoda, 2003). The H3K9me2/3 modification promotes HP1 binding to nucleosomes carrying this modification via its chromodomain that recognizes this mark (Fischle et al., 2003; Jacobs and Khorasanizadeh, 2002). Thus, SUV39H, HP1, and AURKB are part of an epigenetic switch that mediates the transition between a repressive chromatin state (H3K9me2/3 and unmodified H3S10 and H3K14) and a more open active chromatin conformation (H3S10p and H3K14ac) (Liokatis et al., 2012). The repressive combination of H3K9me2/3 and HP1 suppresses transcription of pericentromeric (Lehnertz et al., 2003; Martens et al., 2005) as well as telomeric repeats (Arnoult et al., 2012). In contrast, the relatively rare occurrence of H3S10p during interphase at some genes has been related to enhanced transcription, probably by supporting an open chromatin structure (Ivaldi et al., 2007; Labrador and Corces, 2003; Lee et al., 2006; Lo et al., 2000; Nowak and Corces, 2004). Furthermore, H3S10 phosphorylation was found during S phase for the first two cell divisions in embryogenesis (Teperek-Tkacz et al., 2010) and was linked to replication of heterochromatin in ESCs (Brown et al., 2013).

Here, we set out to investigate if a functional role of H3S10p-mediated repeat transcription exists during interphase in mouse embryonic stem cells (ESCs). We show that the production of centromeric RNA from minor satellite repeats (referred to here as *cen*RNA) is induced during the S phase of the cell cycle by AURKB-dependent H3S10 phosphorylation at subtelomeric regions. The resulting upregulation of *cen*RNA enhances the activity of the reverse transcriptase telomerase in *trans* to maintain telomeric repeats at the chromosome ends. Additionally, we show that AURKB interacts with both *cen*RNAs and TERT, the protein subunit of telomerase. Thus, our study identifies a mechanism by which a histone H3 phosphorylation-methylation switch controls *cen*RNA transcription and telomerase activity in a cell-cycle-specific manner.

RESULTS

AURKB Phosphorylates Centromeric and (Sub)telomeric Loci at Chromosomal p-Arms in ESCs during S Phase

We investigated the H3S10p pattern in mouse ESCs by immunofluorescence using the replication protein factor proliferating cell nuclear antigen (PCNA) as a cell-cycle marker. During the G1 phase, hardly any H3S10p was detectable in ESCs. However, distinct H3S10p foci became clearly visible during S phase adjacent to DAPI-dense regions (Figure 1A). The H3S10p foci persisted during G2 when the characteristic H3S10p pattern in the pericentric heterochromatin regions was established. AURKB

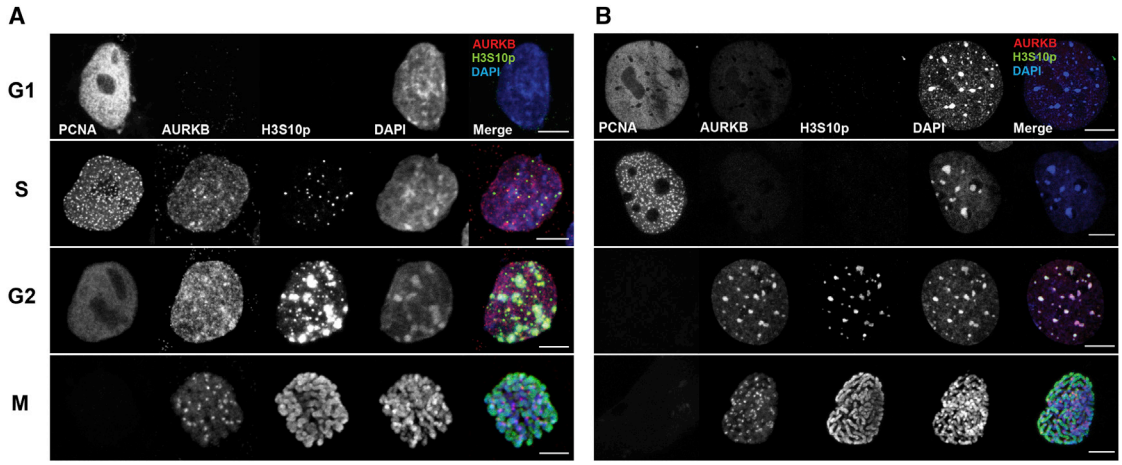

Figure 1. Appearance of H3S10p Domains and AURKB during the Cell Cycle

(A) Representative CLSM images of AURKB and H3S10p distribution in ESCs visualized by immunostaining during the cell cycle. PCNA-GFP was used as a marker for cell-cycle stages, displaying a homogenous distribution in G1 and a punctuate pattern due to the appearance of replication foci in S phase. More than 90% of the ESCs that displayed this S phase PCNA nuclear distribution also had H3S10p foci. At this cell-cycle stage, AURKB was also detected by immunostaining. The H3S10p foci persisted during G2, when H3S10p was enriched at DAPI-dense regions. Color-coding of merged image: H3S10P, green; AURKB, red; DAPI, blue. Scale bars, 5 μm.

(B) Primary MEFs imaged as described for (A). AURKB and H3S10p were restricted to DAPI-dense regions in G2, and both were undetectable in G1 and S phase. Scale bars, 5 μm.

was homogenously distributed throughout the nucleus during S phase as detected by immunostaining in ESCs with enrichments at the H3S10p foci, while the signal was absent during G1 (Figure 1A). In contrast, the dot-like H3S10p distribution in S phase was not detectable in primary mouse embryonic fibroblasts (MEFs) (Figure 1B). In these cells AURKB expression was not detected during S phase but the enzyme became enriched at pericentric heterochromatin in G2 (Figure 1B).

The H3S10p-rich foci observed during S phase in ESCs were centered between the telomere and the centromere on the p-arm of each chromosome as inferred from a three-color staining for CENP-A, as a marker for the centromere and TRF2 to visualize the telomeres (Figure 2A). From the confocal lasers scanning microscopy (CLSM) 3D-image stacks we selected samples that had the p-arm oriented in the x-y plane (Figure 2B, top panel) or aligned along the optical axis/z axis of the microscope (Figure 2B, bottom panel). Comparison of the successive images taken along the z axis showed that the phosphorylation mapped to the chromosome p-arm and covered a region between the centromeres and telomeres that extended into the corresponding repeat sequences. Chromatin immunoprecipitation sequencing (ChIP-seq) of histone H3 and H3S10p showed an enrichment of H3S10p at centromeric repeats, but not at q arm subtelomeres, as inferred from the read distributions for synchronized ESCs (Figures S1A and S1B). In the unsynchronized cells, mitotic H3S10p covered the whole chromosome and dominated the signal with similar values for both regions.

Based on the above results we conclude that the H3S10p foci observed during S phase comprise a part of the centromeres, the subtelomeric regions, and a part of the telomere repeats at the chromosome p-arm. In the following, we refer to them as SPPs for (serine 10 phosphorylated p-arms) (Figure 2C). SPPs were also observed in the widely used Oct4-GiP ESCs (Lowell et al., 2006) that express GFP under the control of the Oct4 promoter and thus seem to be a general feature of mouse ESCs (Figure S1C).

When stem cells were treated with AURKB inhibitors such as reversine or ZM-447439, SPPs were essentially absent after 4 hr of treatment (Figure S1D). At a concentration of 1 μM, the AURKB inhibitor ZM-447439 blocked H3S10 phosphorylation during S phase, but not during mitosis, so that cells proliferated and experiments with long-term AURKB inhibition could be conducted. Under these conditions, ESCs displayed unchanged morphology, *Oct4* expression, and cell-cycle properties for up to 15 weeks (Figures S1E–S1I). In addition, cell-cycle kinetics were comparable as shown by a release from a mitotic arrest (Figure S1J). Thus, at a 1-μM ZM-447439 inhibitor concentration, AURKB was selectively inhibited in S phase in the whole cell population and SPPs were lost without inducing cell-cycle defects, such as anaphase bridges (Figure S2E) or differentiation. The possibility to selectively inhibit AURKB activity at SPPs in S phase at low inhibitor concentrations (Figure S2D) can be rationalized by the increase of AURKB expression from S phase to a maximum in mitosis as shown by fluorescence-activated cell sorting (FACS) (Figures S2A and S2B). In addition, we show that knockdown of AURKB also diminishes H3S10p in S phase in ESCs (Figure S2C). These results demonstrate that SPPs originate from the activity of AURKB acting as both an interphase and a mitotic kinase in ESCs.

Centromeric Transcription Is Regulated by the Interplay of H3K9 Methylation, H3S10 Phosphorylation, and HP1 Binding at SPPs

Since *Suv39h1/h2* double-null (*Suv39h* dn) immortalized mouse embryonic fibroblasts (iMEFs) show an elevated level of H3S10p during interphase (Peters et al., 2001), we analyzed their H3S10p

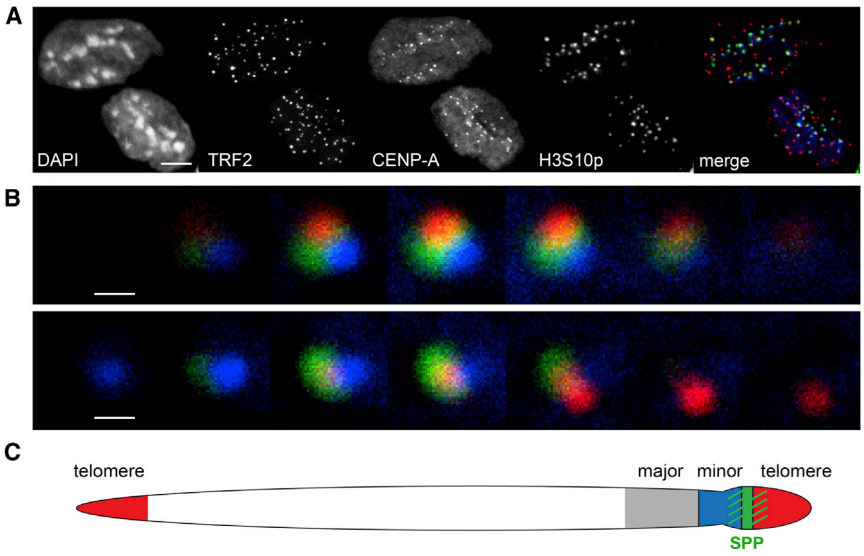

Figure 2. Chromosomal Location of H3S10p Foci in ESCs

(A) Representative CLSM immunofluorescence images of centromere, telomere, and H3S10p in ESCs. Staining of CENP-A (blue) and H3S10p (green) and transfection of RFP-TRF2 (red) showed that the H3S10p foci were located near every centromere. Scale bars, 5 μm.

(B) Stack of enlarged optical sections taken along the optical axis of the confocal microscopy images for two different chromosomes. The upper series shows images, in which H3S10p (green), the centromere (blue), and the telomere (red) are in the same image plane. The bottom series displays a view with the centromere, H3S10p, and the telomere appearing sequentially, i.e., the p-arm chromosome was located perpendicular to the image plane. Scale bars, 0.5 μm.

(C) Scheme for chromosomal location of H3S10p foci. Serine 10 phosphorylated p-arm loci, referred to here as SPPs (green), were located between the centromere (blue) and telomere (red) of the p-arm and partially overlapped with the centromeric and telomeric regions.

See also Figures S1 and S2.

pattern by immunostaining. We detected SPPs in *Suv39h* dn iMEFs that were undistinguishable from those found in ESCs (Figure S3). Next, it was tested whether the SUV39H-mediated H3K9me2/3 modification suppresses phosphorylation of H3S10. To this end, wild-type SUV39H1 or the inactive H324L mutant and PCNA-RFP, a fusion protein of PCNA (proliferating cell nuclear antigen), and red fluorescent protein (RFP), were transfected into ESCs. Then, the number of SPPs was counted and compared to cells transfected only with PCNA-RFP (Figure 3A). The overall number of SPPs was reduced from 23 ± 1 in wild-type cells to 8 ± 1 in *Suv39h1* transfected cells (error bar corresponds to SEM; p value < 0.001, t test) (Figure 3A). The inactive *Suv39h1* mutant did not influence the formation of SPPs. To exclude that the H3S10p antibody is negatively affected by H3K9me3, we assessed its specificity with a histone peptide array (Figure S4A). The results show that the antibody specifically detects H3S10p independent of the absence or presence of adjacent lysine 9 methylation.

HP1 isoforms alpha, beta, and gamma bind to both the centromere and the pericentric major satellite repeats, where its presence correlates with H3K9me3 and chromatin silencing (Fodor et al., 2010; Müller-Ott et al., 2014). HP1 is released during G2 from the (peri)centromeres by the combination of H3S10p and H3K14ac modifications (Fischle et al., 2005; Mateescu et al., 2004). Accordingly, we investigated if H3S10p in SPPs was accompanied by acetylation of lysine 14. We found that this was indeed the case in both ESCs and *Suv39h* dn iMEFs (Figure S4B). Since the combination of H3S10p and H3K14ac is incompatible with HP1 binding, we evaluated the presence of HP1α at SPPs. We found that HP1α-rich foci formed at subtelomeric regions upon AURKB inhibition in S phase (Figures 3B and 3C). Knockdown of AURKB resulted in the same relocalization of HP1α as AURKB inhibition (Figure S4C). In addition, H3K9me3 levels increased at SPPs upon AURKB inhibition (Figure 3B). We conclude that HP1 and H3K9me3 accumulation—two prototypic features of a transcriptionally silent state—were absent in SPPs due to AURKB activity.

Since SPPs were only detectable at the short arm subtelomeric regions, we measured transcript levels from these regions in dependence of the H3S10p state modulated by the inhibition of AURKB with ZM-447439. Transcription of major and minor satellite repeats from the (peri)centromeres as well as the expression of the telomeric RNA TERRA were quantitated by real-time PCR. TERRA levels and major satellite transcripts (*pc*RNA) hardly changed after inhibition of AURKB for 48 hr, whereas minor satellite transcripts from the centromere (*cen*RNA) were reduced by 54% ± 2% (p value < 0.01, t test) (Figure 3D). Absence of genomic DNA was confirmed by real-time PCR (Figure S4D). Since it was reported that centromeric transcripts are double stranded (Martens et al., 2005), we also checked strand-specific changes of *cen*RNA levels. Via cDNA synthesis with primers for the forward and the reverse transcript and subsequent real-time PCR quantification a reduction of both transcripts by ~50% (p value < 0.05, t test) upon AURKB inhibition was measured (Figure 3E).

Expression of *cen*RNA was followed through the cell cycle by synchronizing the ESCs with aphidicolin in G1. ESCs had hardly progressed 2 hr after released from the cell-cycle arrest, and the majority still resided at the G1/S border (Figure S4E). After 5 hr, most cells had entered S phase, and some had proceeded into G2. The presence of ZM-447439 did not affect cell-cycle progression (Figure S4E). The transcription level of the centromeric repeats was measured by real-time PCR relative to that of the control cells and normalized to *Gapdh* transcripts (Figure S4F). When AURKB was inhibited, *cen*RNA expression was independent of cell-cycle progression. Without the inhibitor, *cen*RNA expression reached its maximum 5 hr after release, which was 1.7-fold higher than in arrested cells and 2.5-fold higher than in

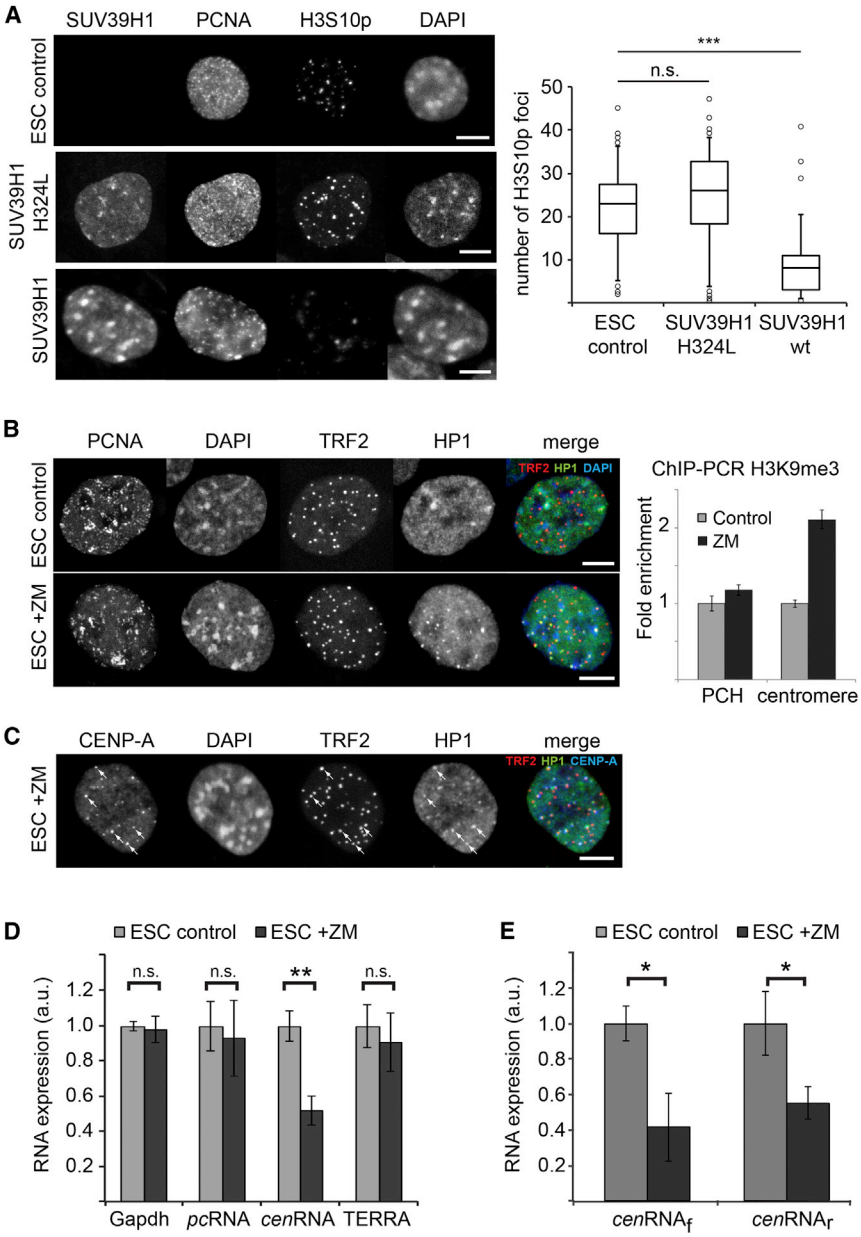

Figure 3. Analysis of H3S10p, SUV39H1 Activity, HP1 Binding, and *cen*RNA Expression

(A) CLSM images of H3S10p in ESCs overexpressing SUV39H1. ESCs were transfected with plasmids for overexpression of GFP-tagged WT SUV39H1 or the catalytically inactive H324L mutant and PCNA-RFP or only with PCNA-RFP and stained for H3S10p. Scale bar, 5 μm. The box plot displays the quantification of the H3S10p foci. Most cells transfected with *Suv39h1* showed approximately eight H3S10p foci in S phase, whereas more than 23 foci were counted in control cells residing in S phase ($n > 70$). See also Figure S3 for SPPs in *Suv39* dn cells and Figure S4A for specificity of the H3S10p antibody used here.

(B) HP1 distribution in ESCs after AURKB inhibition. In ESC control cells, HP1 showed some enrichment at DAPI-dense regions and was otherwise homogenously distributed. Upon AURKB inhibition, HP1 formed distinct foci in S phase. In the merged image HP1 is shown in green, TRF2 in red, and DAPI in blue. Scale bars, 5 μm. ChIP-PCR shows enrichment of H3K9me3 at centromeres, but not at pericentric heterochromatin (PCH) after AURKB inhibition. Error bars correspond to the SD of three independent replicates. See also Figure S4C for siRNA knockdown of AURKB.

(C) Localization of HP1 foci induced by AURKB inhibition. Sites with HP1 enrichment were located at the p-arm and overlapped with centromeres and telomeres (see white arrows) like the SPPs that were lost due to AURKB inhibition. In the merged image HP1 is shown in green, TRF2 in red, and CENP-A in blue. Scale bar, 5 μm.

(D) RNA quantification after AURKB inhibition by real-time PCR. Values were normalized using β-actin, while *Gapdh* served as an internal control. A reduction of *cen*RNA in ZM-447439-treated cells was observed after 48 hr. Error bars correspond to the SD of three independent replicates. See also Figure S4D confirming the absence of genomic DNA.

(E) Strand-specific real-time PCR of *cen*RNA. Both $cenRNA_f$ and $cenRNA_r$ transcripts were reduced upon AUKRB inhibition. Error bars correspond to the SD of three independent replicates.

See also Figures S4E and S4F for cell-cycle-dependent *cen*RNA expression.

ZM-447439-treated cells after release (p value < 0.05, t test). Thus, *cen*RNA expression was highest during S phase and dependent on AURKB.

AURKB Inhibition Leads to Telomere Shortening due to Lack of *cen*RNA

It has been shown that chromatin organization plays an important role in telomere maintenance (Blasco, 2007). As SPPs were located near the p-arm telomere and are needed for an open chromatin structure, we investigated whether SPPs and AURKB activity had an effect on telomere repeat maintenance at the p-arm. We determined total telomere length by fluorescence in situ hybridization against the telomere repeats coupled with flow cytometric quantification (flow-FISH). H3S10 phosphorylation was blocked in S phase with ZM-447439 for up to 15 weeks. Wild-type ESCs were compared with ZM-447439-treated cells after 4 and 15 weeks and wild-type cells that were cultured for 15 weeks in the absence of the AURKB inhibitor. The telomere length remained unchanged for untreated ESCs during this period. However, the ZM-447439-treated cells displayed a progressive telomere shortening over time (Figure 4A). After 4 weeks, telomeres were shortened by 6% ± 3% and by 11% ± 2% after 15 weeks. Telomere replication was not affected and still occurred early during the onset of S phase in both treated and untreated cells (Figure S5A).

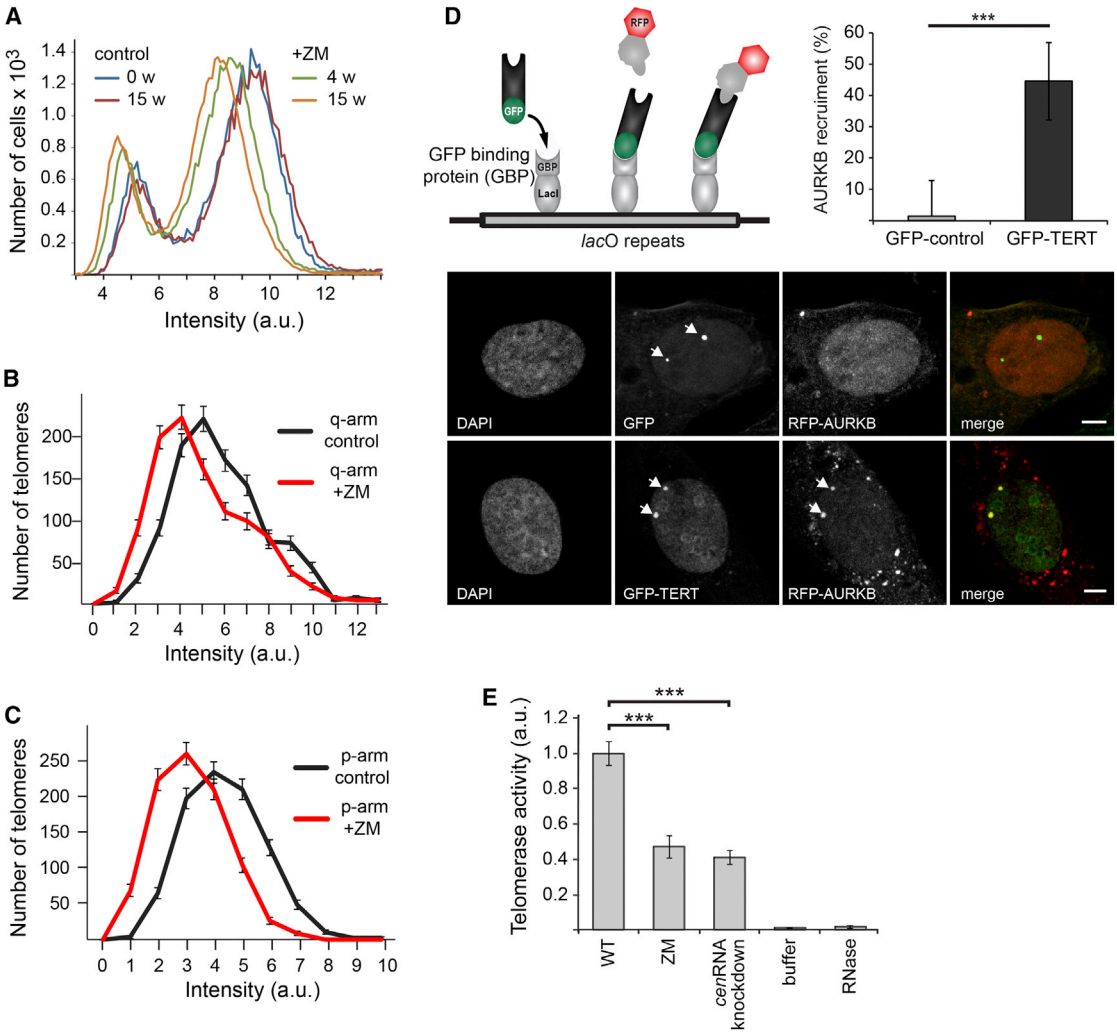

Figure 4. Reduction of Telomerase Activity upon AURKB Inhibition and *cen*RNA Knockdown

(A) Flow-FISH measurements of telomere length. Cells were cultured for up to 15 weeks untreated (control) or treated with ZM-447439 (+ZM). After that period, control cells had the same telomere length distribution as cells at the beginning of the experiment (blue and red line). Time points after 4 weeks (+ZM 4 w, green) and 15 weeks (+ZM 15 w, orange) show progressive loss of telomere signal indicating shortening of telomeres due to treatment with ZM-447439. Average curves calculated from three independent replicates are shown. The two peaks of all curves correspond to cells without (first peak) and with (second peak) replicated telomeres, hence the doubling of the signal intensity. See also Figure S5A for replication timing of telomeres.

(B) Histograms of the telomere probe intensity of the q-arm telomere for ZM-447439 (+ZM) treated and control cells. Error bars correspond to the SD.

(C) Same as (B), but for p-arm telomeres. Both q- and p-arm telomeres showed a shift to lower intensities indicative of loss of repeats upon ZM-447439 treatment. Error bars correspond to the SD.

(D) Recruitment of AURKB by GFP-TERT bound to *lac*O-arrays. GFP-TERT was tethered to *lac*O-arrays in telomerase-negative U2OS cells, and subsequent binding of RFP-AURKB was evaluated. GFP served as a negative control. The bar plot gives the percentage of cells with positive recruitment. RFP-AURKB was clearly enriched when GFP-TERT was tethered to the lacO arrays. Error bars correspond to the SE from more than 50 cells. Scale bars, 5 μm.

(E) Quantification of telomerase activity measured in a quantitative TRAP assay. Telomerase activity was largely reduced by AURKB inhibition and *cen*RNA knockdown. Buffer and RNase-A-treated cell extracts served as negative controls. Error bars correspond to the SD. See also Figure S5 for expression levels of TERT and *TERC*.

Next, telomere length was assessed on metaphase spreads to separately evaluate shortening at the p and q arm of each chromosome. An overall shortening of 15% ± 2% (p value < 0.001, t test) was measured for the ZM-447439-treated cells after 15 weeks as compared to their wild-type controls, which is in excellent agreement with the flow-FISH analysis. Interestingly, both telomeres at p and q arm were shortened (p value < 0.001, t test) (Figures 4B and 4C), indicating that the H3S10p-dependent telomere maintenance mechanism acts in *trans* and not in *cis*. To exclude the possibility, that AURKB activity directly affects expression of telomerase, we confirmed that transcription of *Tert* and *Terc* encoding for the telomerase protein and RNA component, respectively, remained unchanged upon inhibition of AURKB (Figures S5B and S5C). Furthermore, we

prepared two independent RNA-sequencing (RNA-seq) libraries from wild-type as well as from AURKB inhibitor-treated cells. Differential expression analysis with the DESeq software identified ten upregulated and no downregulated genes at the $p < 0.01$ significance level (Table S1). None of the upregulated genes had any apparent link to the observed interference with telomere maintenance.

We next tested in living cells if AURKB and TERT interact with each other, which might indicate a direct link between AURKB inhibition and telomere shortening. Mouse GFP-tagged TERT was tethered to *lac*O-arrays integrated at two chromosomes in a human U2OS cell line as described previously (Chung et al., 2011). This led to a strong enrichment of RFP-AURKB at the two loci with tethered GFP-TERT (Figure 4D). In contrast, tethering only the GFP protein did not recruit AURKB. This demonstrates that AURKB interacts with TERT in living cells.

To examine whether telomerase activity was impaired by either AURKB inhibition or depletion of *cen*RNA, we measured telomerase activity with a quantitative telomeric repeat amplification protocol (TRAP) assay (Herbert et al., 2006). We compared wild-type cells with ZM-447439-treated cells and cells transfected with two chimeric RNA-DNA oligomers for *cen*RNA knockdown by RNase-H-mediated degradation (Liang et al., 2011). One of these antisense oligonucleotides targeted the minor satellite forward transcript (*cen*RNA$_f$), while the other was complementary to the reversely transcribed RNA (*cen*RNA$_r$). Transfection with the two knockdown oligonucleotides resulted in a 70% reduction of *cen*RNA (p value < 0.001, t test) as measured by real-time PCR (Figure S6A). Both AURKB inhibition and *cen*RNA knockdown led to a reduction of telomerase activity of 50% and 40%, respectively (p value < 0.001, t test) (Figure 4E). The linear relationship between protein content and telomerase activity and dynamic range of the TRAP analysis is depicted in Figure S6B.

Interestingly, the *Suv39h* dn iMEFs showed a 22-fold higher expression level of *cen*RNA as compared to wild-type iMEFs (p value < 0.001, t test) (Figure S5D). In contrast, the *Tert* expression level was 22-fold lower in the *Suv39h* dn than in wild-type iMEFs (p value < 0.001, t test), while *Terc* expression and telomerase activity were similar in both cell types (Figures S5D and S5E). Accordingly, we speculate that telomerase activity in *Suv39h* dn cells is maintained by overexpression of *cen*RNA and AURKB (Figure S5D) to compensate for the much lower TERT levels.

Telomerase Activity Loss Can Be Rescued by Ectopic *cen*RNA Expression

Since it was previously reported that *cen*RNA can enhance AURKB activity (Ferri et al., 2009), we extended the *cen*RNA$_f$ and *cen*RNA$_r$ sequences with an RNA fragment that contained eight MS2 stem loops. The resulting MS2-*cen*RNA$_f$ and MS2-*cen*RNA$_r$ constructs were tethered to *lac*O-arrays via a fusion construct of LacI-RFP with the MS2 binding protein (LacI-RFP-MS2). Both MS2-*cen*RNA$_f$ and MS2-*cen*RNA$_r$ tethered to the *lac*O integration sites induced a clear recruitment of GFP-AURKB to these loci (Figure 5A). In contrast, binding of only the MS2 stem loop containing RNA to the *lac*O-arrays did not lead to an enrichment of GFP-AURKB. Based on these findings, we propose that the *cen*RNA-mediated enhancement of telomerase activity in ESCs occurs via interactions of a *cen*RNA-AURKB complex with the TERT subunit of telomerase. It is noted that this mechanism explains how AURKB inhibition and subsequent repression of *cen*RNA transcription via epigenetic silencing affects telomere repeat extension in *trans*.

To corroborate the functional relationship of *cen*RNAs and AURKB for regulating telomerase activity, we tested whether telomerase activity could be rescued by overexpression of these RNAs after AURKB inhibition. To this end, we cloned the minor satellite repeat sequence in an expression vector with an RNA polymerase III promoter and transfected AURKB inhibited cells twice over 48 hr. Expression of *cen*RNA was increased 3.5-fold and 1.8-fold over the mock control (empty vector) in transfected wild-type cells for the forward and reverse transcripts, respectively (Figures S6C and S6D). Telomerase activity was compared between wild-type cells and ZM-447439-treated cells. ZM-447439-treated cells were either untransfected or transfected with the empty vector (“Mock”) or *cen*RNA$_f$ and *cen*RNA$_r$ expression constructs (Figure 5B). Only cells expressing *cen*RNA$_f$ and *cen*RNA$_r$ simultaneously showed a significant rescue of telomerase activity compared to mock transfection and untransfected ZM-447439-treated cells. Thus, we conclude that the active form of *cen*RNA is double stranded.

Next, we in vitro translated AURKB and TERT and performed in vitro phosphorylation of TERT by AURKB. The telomerase activity was measured in the absence or presence of wild-type AURKB or inactive mutants, *cen*RNA, and major satellite RNA from the pericentromeric repeats. Telomerase activity was elevated by AURKB alone, but not by inactive AURKB mutants. It further increased by the addition of *cen*RNA, but not by the *pc*RNA repeat sequence of similar length from the major satellite repeat (Figure 5C). We conclude that *cen*RNA acts as an enhancer of an AURKB-mediated telomerase activation.

DISCUSSION

Centromeric minor satellite repeat sequences are actively transcribed to yield double-stranded transcripts of heterogeneous length from 25 up to several thousand base pairs, depending on the activity of the endoribonuclease Dicer (Kanellopoulou et al., 2005; Martens et al., 2005). The overexpression of these RNAs referred to here as *cen*RNAs induce a chromosome segregation defect phenotype (Bouzinba-Segard et al., 2006), but their specific cellular activities have remained enigmatic. Here, we show that AURKB-driven histone H3 serine 10 phosphorylation enhances *cen*RNA expression in mouse ESCs during the S phase of the cell cycle.

Since all mouse chromosomes are acrocentric, the centromeres are adjacent to the short arm telomere, with only a small variable linker region separating these two chromosomal regions (Guenatri et al., 2004; Kalitsis et al., 2006; Sasaki et al., 2013). The center of the H3S10p-rich SPP loci was mapped by CLSM analysis to this subtelomeric region between the centromere and the telomere on the p-arm of each mouse chromosome but also extended to the flanking parts of the genome. ChIP-seq analysis of H3S10p showed that H3S10p was also enriched at the centromeric repeats themselves. Since inhibition of H3S10p affected only the transcription of the centromere

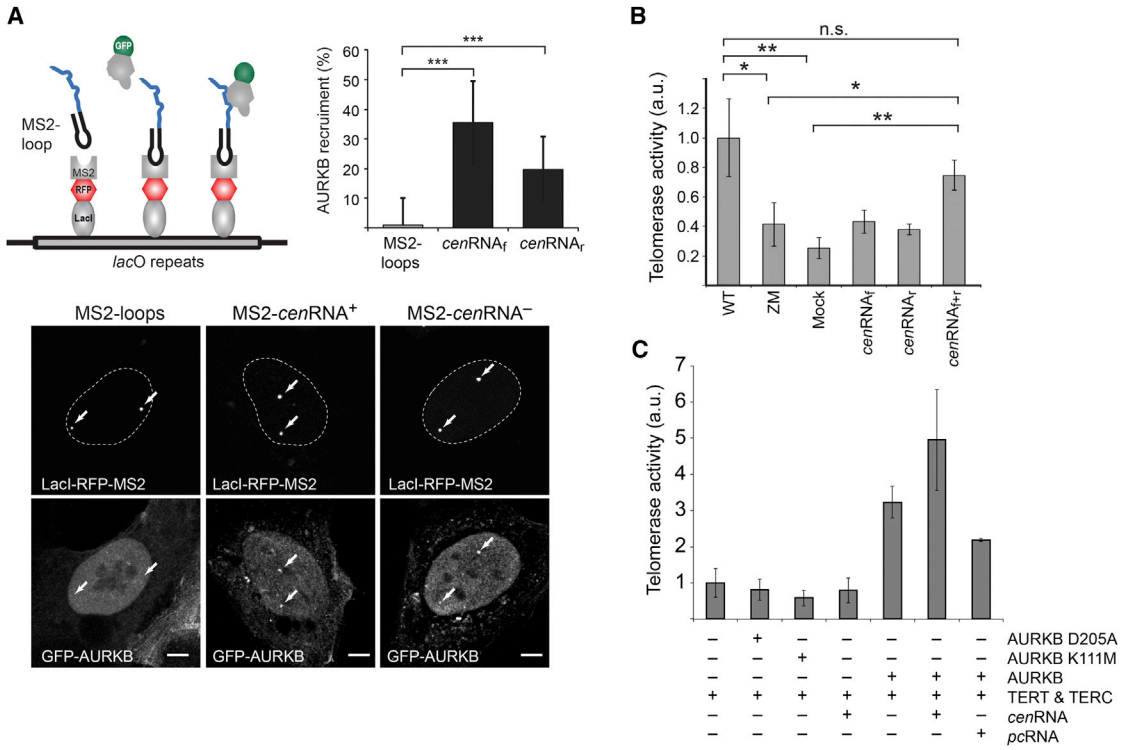

Figure 5. Interaction of *cen*RNA with AURKB and Telomerase Activity Enhancement

(A) Recruitment of AURKB by *cen*RNAs bound to *lac*O-arrays. MS2-*cen*RNA was tethered to *lac*O-arrays by the LacI-RFP-MS2-coat fusion protein. The bar plot gives the percentage of cells with positive recruitment. Recruitment of GFP-AURKB was observed with both MS2-*cen*RNA$_f$ and MS2-*cen*RNA$_r$, whereas MS2 stem loops did not induce an enrichment of GFP-AURKB. The dashed line in the upper row indicates the position of the nucleus. Error bars correspond to the SE from more than 50 cells. Scale bars, 5 μm.

(B) Rescue of telomerase activity by *cen*RNA overexpression measured in a TRAP assay. While transfection with an empty plasmid showed no effect, simultaneous expression of *cen*RNA$_f$ and *cen*RNA$_r$ resulted in partial rescue of telomerase activity. Error bars correspond to the SD of three replicates. See also Figure S6 for overexpression of *cen*RNAs.

(C) Telomerase activity is increased by AURKB and *cen*RNA. AURKB, TERT, and RNAs were in vitro translated and assembled in a phosphorylation buffer, and telomerase activity was measured in a TRAP assay. Activity was highest when TERT and TERC were mixed with AURKB and *cen*RNAs. Error bars correspond to the SD of three replicates.

repeats, but not that of major repeats or telomeric transcripts, we speculate that the SPPs contain promoter and/or enhancer regions for *cen*RNAs and that the phosphorylation also contributes to a transcription permissive chromatin structure within the repeats. Activation of their transcription by H3S10p could also involve H3K14ac, which was found to be associated with H3S10p in SPPs. Similar to the molecular events that occur during mitosis (Fischle et al., 2005), HP1 became depleted from SPPs by the H3S10p and H3K14ac histone modifications, which is likely to promote transcription of the centromeric repeats. In contrast, AURKB inhibition resulted in HP1 binding to this region and silencing of *cen*RNA expression. The formation of SPPs was counteracted by the activity of SUV39H-driven H3K9 di/trimethylation as concluded from *Suv39h* dn fibroblasts having SPPs and high levels of *cen*RNA and the reduction of SPPs/H3S10p levels upon overexpression of SUV39H1 in ESCs.

Thus, the previously described network of SUV39H1/2-driven H3K9 di/trimethylation, the recognition of this modification by HP1, and the counteracting process of H3S10 phosphorylation followed by H3K14 acetylation operate in mouse ESCs to regulate *cen*RNA transcription during the S phase of the cell cycle. Upregulating *cen*RNA by this histone phosphorylation-methylation switch is of functional importance, since it is required for efficient telomere elongation. This is consistent with the finding that telomerase is mostly active during S phase after the telomeres have already been replicated (Jády et al., 2006; Tomlinson et al., 2008; Zhao et al., 2008).

Interestingly, it has been reported previously that telomerase processivity is affected by posttranslational histone modifications. Telomeric chromatin in differentiated mouse cells lacking telomerase activity is in a repressive heterochromatic state that is characterized by histone H3K9me3 and binding of HP1 (Benetti et al., 2007b; García-Cao et al., 2004). Depletion of the histone methylases SUV4-20H1/H2 (catalyzing H4K20me3) and SUV39H1/H2 leads to aberrant telomere elongation (Benetti et al., 2007a, 2007b). At the same time, overexpression of SUV39H1 in mice results in telomere shortening (Petti et al., 2015), which is in line with the finding reported in our study on suppression of SPPs and *cen*RNA expression by enhanced SUV39H1 activity.

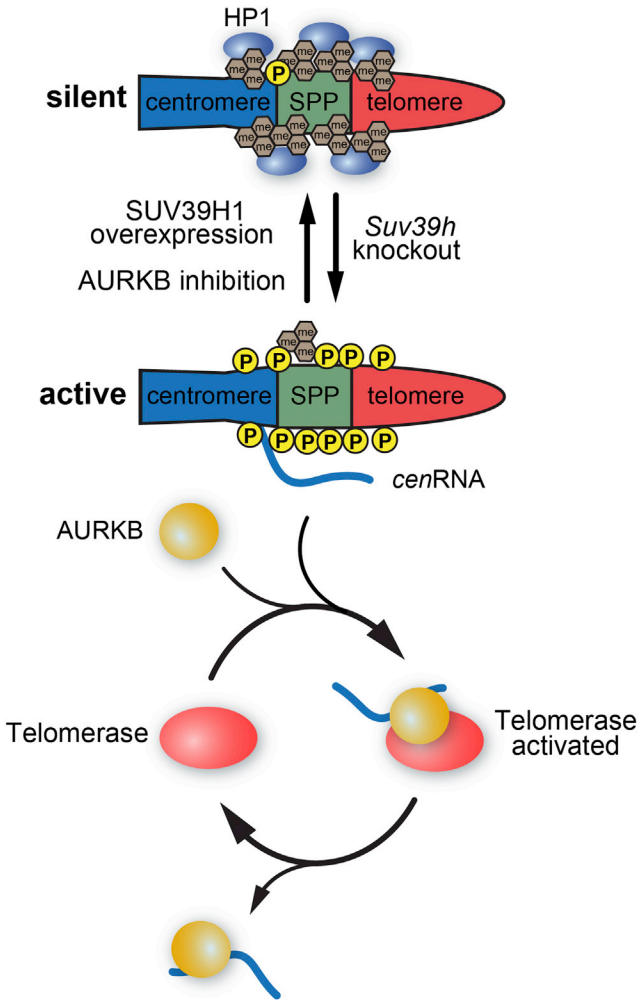

Figure 6. Model for Telomerase Activation by *cen*RNA via a Histone Phospho-Methylation Switch

AURKB expression leads to the formation of SPPs between the centromere and telomere, which induces *cen*RNA expression. In turn, *cen*RNAs bind to AURKB and this complex interacts with TERT to enhance telomerase activity needed for efficient telomere elongation. Telomerase activation is impaired by AURKB inhibition and *cen*RNA knockdown. In addition, SUV39H activity promotes H3K9me3 and HP1 binding to induce a chromatin state that counteracts H3S10p formation during S phase and silences *cen*RNA expression.

In mouse ESCs, however, the telomeres lack these typical heterochromatin markers and telomerase is active. Induction of a heterochromatic chromatin state at SPPs by AURKB inhibition did affect telomere repeat extension in *trans* as shown by the telomere intensity analysis (Figures 4B and 4C). Furthermore, we identified a specific mechanism in ESCs, by which SUV39H, H3K9me3, and HP1 counteracted the transcriptionally active chromatin state that was established during S phase via the H3S10p modification. In the active state, the extension of telomere repeats by telomerase was promoted via upregulation of *cen*RNA. Both AURKB inhibition and the knockdown of *cen*RNA resulted in a less active telomerase complex (Figure 4E). This conclusion is supported by the previously reported finding that knockdown of AURKB results in a reduced telomerase activity in human cancer cell lines (Cerone et al., 2011). In the latter study, however, it remained unclear, whether this effect resulted from mitotic defects and/or cell-cycle arrest. In our study, AURKB was selectively inhibited in S phase and cell division was not impaired, and hence we can rule out cell-cycle effects on telomerase activity. Additionally, we did not observe changes in *Tert* or *Terc* expression when AURKB was inhibited.

Notably, long-term inhibition of AURKB resulted in a constant loss of telomere repeats in ESCs. Interestingly, *Suv39h* dn iMEFs had a 22-fold reduced *Tert* level, while the level of *cen*RNA was 22-fold increased as compared to the wild-type fibroblasts. This finding suggests that a low level of *Tert* expression was sufficient to ensure immortalization of *Suv39h* dn embryonic fibroblasts, as the higher *cen*RNA and AURKB levels in S phase provides sufficient telomerase activation at relatively low TERT concentrations. In this manner, a telomerase activity level could be obtained for *Suv39h* dn cells that was comparable to the wild-type immortalized fibroblasts.

In-vitro-translated telomerase was more efficient in the TRAP assay in combination with AURKB. This clearly shows that AURKB can indeed accelerate telomerase activity. In contrast to RNA from major satellite repeats, in-vitro-transcribed *cen*RNA further increased telomerase activity. This is fully consistent with our observation of reduced telomerase activity after knockdown of *cen*RNA (Figures 4E and 5C), while the overexpression of *cen*RNA partially rescued the loss of telomerase activity upon AURKB inhibition (Figure 5B).

Our findings link *cen*RNA, AURKB, and TERT activity and are summarized in the scheme depicted in Figure 6. After replication of telomeres, H3S10 phosphorylation by AURKB induces *cen*RNA expression during S phase. Via interaction of the *cen*RNA-AURKB complex with TERT, the telomerase complex is activated in *trans* to compensate the loss of telomere repeats that occurred during replication. This activation step could involve the formation of telomerase dimers, which have been proposed to be more active in such a complex (Wenz et al., 2001) and/or an increase the enzyme's processivity by phosphorylation of TERT. Phosphorylation of TERT, e.g., by Akt, has been associated with telomerase activity (Haendeler et al., 2003; Seimiya et al., 1999), whereas dephosphorylation by protein phosphatase 2A inhibits TERT in vitro (Li et al., 1997; Xi et al., 2013). It is thus conceivable that AURKB regulates TERT activity by phosphorylation. Since *cen*RNA also enhances AURKB activity (Ferri et al., 2009), the underlying network could include a feedback loop in which these transcripts further promote H3S10p formation. SUV39H promotes a chromatin state in which H3K9me3 and HP1 binding suppress H3S10p and *cen*RNA expression as inferred from the analysis of *Suv39h* dn cell and overexpression of SUV39H1. Thus, via regulating *cen*RNA expression by a cell-cycle-dependent histone modification switch, telomerase activity in mouse ESCs is synchronized with telomere replication. Modulating telomerase activity in this manner has a number of implications for tumorigenesis as well as reprogramming of somatic cells, since activation and regulation of telomere maintenance is a crucial step in both processes. Therefore, we anticipate that investigating the role of the epigenetic network revealed here in other cellular systems will

Table 1. Primers Used for Real-Time PCR

Target	Sequences in the 5′-3′ Direction
Telomere fwd	CGGTTTGTTTGGGTTTGGGTTTGGGTTTGGGTTTGGGTT
Telomere rev	GGCTTGCCTTACCCTTACCCTTACCCTTACCCTTACCCT
*cen*RNA$_f$	AATGATAAAAACCACACTGTAGAACAT
*cen*RNA$_r$	ATGTTTCTC ATTGTAACTCATTGATATAC
Major repeat fwd	TGGCGAGAAAACTGAAAATCACG
Major repeat rev	TCTTGCCATATTCCACGTCCTAC
β-Actin fwd	TATCCTGACCCTGAAGTACC
β-Actin rev	CTCGGTGAGCAGCACAGGG
Gapdh fwd	TATGTCGTGGAGTCTACTGG
Gapdh rev	ACACCCATCACAAACATGGG
Tert fwd	TAGAGGATTGCCACTGGCTCC
Tert rev	AGCTGTACCACGTATGTGTCC
Terc fwd	GGTTCTGGTCTTTTGTTCTCCG
Terc rev	TTTTGAGGCTCGGGAACGCG

provide valuable information on the linkage between changes of (sub)telomeric and/or centromeric chromatin and functional cell states via *cen*RNA effector transcripts.

EXPERIMENTAL PROCEDURES

Cell Culture

129/Ola ESCs (Mallm et al., 2010) used for this study were cultured in Powerstem ESPRO1 (PAN) on gelatin-coated surfaces. GIP-ESCs were maintained in ESGRO complete (Millipore) without feeders on gelatin. 129/Ola-Hsd MEFs were generated from pregnant embryonic day 13.5 (E13.5) mice and cultured in DMEM supplemented with 10% fetal calf serum and glutamine up to passage five. The same medium was used to culture SUV39H1/h2 double-null cells and wild-type iMEFs (Peters et al., 2001).

Immunofluorescence and Western Blotting

For immunostaining and transfection, cells were seeded on Matrigel-coated coverslips. Vectors for overexpression of RFP-TRF2, GFP-PCNA, RFP-PCNA, GFP-SUV39H1, and the GFP-SUV39H1 H324L inactive mutant were transfected with lipofectamine 2000. Fixed and stained cells were mounted with Prolong containing DAPI (Invitrogen) and examined using a Leica TCS SP5 confocal laser-scanning microscope equipped with a 63×/1.4 numerical aperture oil-immersion objective lens (Leica Microsystems CMS). For AUKRB knockdown, small interfering RNA (siRNA) (Ambion, s74513) was transfected with lipofectamine 3000 and cells were fixed 36 hr after transfection.

For immunostaining and western blots, the following antibodies were used: AURKB (6/AIM-1, BD Bioscience), CENP-A (2048, Cell Signaling), GAPDH (AM4300, Ambion), histone H3S10p (ab14955, Abcam, for all experiments except immunofluorescence with AURKB, when ab5176 [Abcam] was used), histone H3S10pK14ac (07-081, Millipore), HP1-alpha (2HP-1H5, Euromedex), OCT4 (ab279985, Abcam), TERT (H-231, Santa Cruz). The specificity of the ab14955 H3S10p antibody was verified with the "MODified Histone Peptide Array" (Active Motif) according to the manufacturer's instructions (Figure S4A).

Counting of H3S10p foci after transfection with GFP-SUV39H1 and GFP-SUV39H1H324L mutant was done using ImageJ software. First, the background of the H3S10p staining in the nucleus was determined and a threshold was applied, which was three times higher then the background. Then, H3S10p foci were automatically detected within the nucleus with the constraint that their size had to be in the range from 0.05 to 2 μm^2.

Total RNA Extraction and Real-Time PCR

Total RNA was extracted with the RNeasy kit (QIAGEN) following the manufacturer's instructions. Total RNA was subsequently digested with DNase I for 1 hr to ensure depletion of contaminating genomic DNA. 2 μg total RNA was used for cDNA first-strand synthesis using superscript II reverse transcriptase (Invitrogen), which was followed by RNase H treatment. For quantification, a cDNA standard was prepared that included five samples ranging from 25 ng/μl to 0.35 ng/μl. The standard curve was determined from real-time PCR with 2 μl of each concentration using the SYBR Green I kit by Roche and the StepOne RT-PCR system (Applied Biosystems) and subsequently used to quantify the target cDNA. The following program was used for amplification: 95°C for 10 min followed by 35 cycles with 95°C, 60°C, and 72°C each for 10 s. Three biological independent samples were used for each primer pair with three replicates. *Gapdh* was used for normalization, and β-actin served an internal control. Errors given in the graphics correspond to SEM.

Primers used for real-time PCR are listed in Table 1.

Cell-Cycle and Telomere-Length Flow-FISH Analysis by FACS

For cell-cycle analysis, cells were harvested and fixed with 70% ethanol for 2 hr on ice. After resuspension in staining buffer (PBS containing 100 μg/ml RNase and 0.5 μM TO-PRO3), cells were analyzed with FACS Canto II. Cell-cycle stages were fitted to DNA content profiles with the Weasel flow cytometry data analysis software. For flow-FISH, cells were permeabilized with 0.25% Triton after ethanol fixation. Cells were washed with a buffer containing 5% glucose, 10 mM HEPES (pH 8.0), and 0.1% BSA and were resuspended in hybridization buffer (75% deionized formamide, 20 mM Tris-HCl [pH 7.4], 20 mM NaCl, and 0.1% BSA) with 55 nM PNA (peptide nucleic acid) fluorescein isothiocyanate telC probe (Pangene). After 15 min at 87°C, hybridization was allowed for 90 min at room temperature, and cells were subsequently washed with a buffer containing 70% formamide, 0.1% BSA, 0.1% Tween-20, and 20 mM Tris-HCl (pH 7.4) three times and then washed with a buffer containing 5% glucose, 10 mM HEPES (pH 7.4), 0.1% BSA, and 0.1% Tween-20. Cells were resuspended in staining buffer and analyzed the same day. For each sample, three independent hybridizations were performed.

Protein expression of AURKB was measured by fixing cells with 1% paraformaldehyde (PFA) for 10 min on ice, followed by ethanol fixation for 2 hr. After permeabilizing with 0.25% Triton, the AURKB antibody was diluted 1:200 in 1% BSA/PBS and incubated overnight followed by an Alexa 488 secondary antibody. Cells were resuspensed in staining buffer (PBS containing 100 μg/ml RNase and 0.5 μM TO-PRO3) and analyzed with FACS Canto II.

For synchronization and release from a mitotic block, cells were arrested with 200 nM nocodazole for 24 hr and released by three washes and maintenance in medium.

Metaphase Spreads and Telomere FISH

Colcemid was added to the medium to a concentration of 0.02 μg/ml for 2 hr. Cells were washed and incubated in 0.5% KCl and then fixed in methanol and glacial acetic acid. Fixed nuclei were spotted in coverslips and washed with ethanol. Cell nuclei were incubated with telomere PNA probes at 80°C for 3 min after sealing the coverslips with Fixogum. Hybridization took place overnight. After washes with 70% formamide, 2× SSC buffer (300 mM sodium chloride and 30 mM sodium citrate), 0.1× SSC at 55°C, and 0.05% Tween in 2× SSC, metaphase spreads were dried with ethanol and eventually mounted with Prolong (Invitrogen). For wild-type and inhibitor-treated cells, a minimum of 2,000 telomeres were analyzed from two technical replicates. Pictures were taken at the same day with the same laser settings. Pixel intensities of telomere probes were measured with ImageJ.

RNA-Seq

Total RNA was purified as described above. Ribosomal RNA was removed with the RiboZero kit (Epicenter) following the manufacturer's instructions. After fragmentation with the RNA Fragmentation Reagent (Ambion), cDNA was generated with random primers and superscript II reverse transcriptase (Invitrogen). After second-strand synthesis, the fragments were cloned into an Illumina sequencing library according to standard protocols. Two biologically independent samples of wild-type and treated cells were submitted for sequencing. After mapping with bowtie, differential expression was calculated

with DESeq that was incorporated in the Genomatix software suite as described previously (Teif et al., 2012).

ChIP-Seq of H3S10p

ESCs were synchronized with 3 μg/ml aphidicolin for 20 hr. The cells were released for 3 hr and subsequently cross-linked with 1% PFA. Cell nuclei were prepared using a swelling buffer (25 mM HEPES [pH 7.8], 1 mM $MgCl_2$, 10 mM KCl, 0.1% NP-40, and 1 mM DTT). Chromatin was sheared to mononucleosomal fragments with a Covaris S220 sonicator. After immunoglobulin G preclearance, the sheared chromatin was incubated with 4 μg of either H3S10p (ab14955, Abcam) or histone H3 (ab4729, Abcam) antibody and magnetic protein G beads overnight. The beads were washed with sonication buffer (10 mM Tris-HCl [pH 8.0], 200 mM NaCl, 1 mM EDTA, 0.5% N-lauroylsarcosine, and 0.1% Na-deoxycholate), high-salt buffer (50 mM HEPES [pH 7.9], 500 mM NaCl, 1 mM EDTA, 1% Triton X-100, 0.1% Na-deoxycholate, and 0.1% SDS), lithium buffer (20 mM Tris-HCl [pH 8.0], 1 mM EDTA, 250 mM LiCl, 0.5% NP-40, and 0.5% Na-deoxycholate), and 10 mM Tris-HCl (pH 6.8). Next, chromatin was eluted from the protein G magnetic beads and the crosslink was reversed overnight at 65°C. After RNase A and proteinase K digestion, the DNA was purified and cloned into a multiplexed Illumina library according to standard protocols. Sequenced 50-bp reads were mapped to the mm9 assembly with customized bowtie indices. The number of mapped reads was normalized to the total number of reads.

Quantification of Telomerase Activity with the TRAP Assay

Cells were harvested and lysed in TRAP lysis buffer for 30 min, which contained 10 mM Tris-HCl (pH 7.4), 1 mM $MgCl_2$,1 mM EDTA, 1% (v/v) NP-40, 0.25 mM sodium deoxycholate, 10% (v/v) glycerol, 150 mM NaCl, 5 mM mercaptoethanol, and 1 U/μl Ribolock RNase inhibitor (Fermentas). After centrifugation, the supernatant was collected and total protein concentration was measured using the BCA assay (Thermo Scientific). A standard was prepared that ranged from 0.125 ng/μl to 0.004 ng/μl total protein, and the samples were diluted in lysis buffer to gain a concentration of 0.04 ng/μl. For each TRAP reaction, 2 μl of the lysate were incubated with SYBR Green PCR master mix kit (Applied Biosystems), 5 ng/μl TS primer (5′-AATCCGTCGA GCAGAGTT-3′), 5 ng/μl ACX primer (5′-GCGCGGCTTACCCTTACCCTTACCCT AACC-3′), 1 mM EGTA, and 1 U/μl Ribolock for 30 min at 30°C. PCR was then run for 35 cycles with 15 s at 95°C and 60 s at 60°C.

The measured PCR threshold cycle (Ct) was transformed into an activity value according to the standard curve. This allowed relative quantification of the cell lysates with equal total protein concentration. Errors are given as the SD of the three biological replicates, and the Student's t test was used for statistical testing.

For rescue experiments, cells were treated with the AURKB inhibitor for 48 hr, then seeded on gelatin-coated 12-well plates and transfected with the pBS/U6 plasmids (Grimm et al., 2006) within 3 hr. The *cen*RNAs were cloned into the pBS/U6 plasmid via the Bbs I cloning site in both forward and reverse directions. Expression of GFP from the same plasmid under the CMV promoter was used to judge the transfection efficiency. The amount of *cen*RNA was determined by PCR as described above. For each sample, three biological replicates were performed. At 48 hr after transfection, cells were harvested and subjected to a quantitative TRAP assay.

Knockdown of *cen*RNA

For *cen*RNA knockdown, cells were transfected with RNA-DNA hybrid oligonucleotides that consisted of five to six 2′-O-MOE modified ribonucleotides (shown in capital letter below) flanked by 14 deoxyribonucleotides with a phosphorothioate backbone at the 5′ and 3′ end. For knockdown of $cenRNA_f$ the sequence UGUAGaacagtgtatatcaAUGAG was used while the $cenRNA_r$ knockdown was conducted with the UCAUCUaatatgttctacagUGUGGU oligonucleotide. The two oligonucleotides used for knockdown were not complementary to each other and were transfected into ESCs with Lipofectamine 2000 at a final concentration of 50 nM each. Knockdown efficiency was determined with real-time PCR of reverse-transcribed total RNA.

Protein and RNA Recruitment and Interaction Analysis

GFP-tagged TERT was recruited via a LacI repressor-GFP binding domain fusion protein to *lac*O-arrays integrated in telomerase-negative U2OS cells as described previously (Chung et al., 2011; Jegou et al., 2009). Co-recruitment of RFP-AURKB was measured 24 hr after transfection. Cells were fixed and mounted with Prolong antifade reagent (Life Technologies). Images were taken with a Leica SP5 microscope, and pictures were analyzed with ImageJ. Signal intensity of RFP-AURKB was measured at *lac*O arrays and regions adjacent to the *lac*O arrays. Positive recruitment was defined as the signal increase at the *lac*O array by >1.5-fold as compared to adjacent regions. EGFP recruited to *lac*O-arrays was used as a negative control. For RNA recruitment experiments, one centromere repeat was fused to eight MS2 stem loops in forward and reverse orientation. The fusion construct LacI-RFP-MS2-coat protein was transfected with the tagged centromere repeats and GFP-AURKB. Cells were fixed and imaged as described above. For statistical analysis of AURKB recruitment either by TERT or by *cen*RNA, the Fisher's exact test was used.

In Vitro Phosphorylation of TERT

Open reading frames of AURKB and TERT were cloned into pET28(a)+ and used for in vitro translation with rabbit reticulocyte lysates (RLL; Promega). For in vitro translation of AURKB, 1 μg of plasmid was used, and for TERT, 1.5 μg plasmid plus 250 ng in-vitro-transcribed TERC was used and incubated according to the manufacturer's instructions. AURKB mutants K111M and D205A were generated by site-directed mutagenesis.

Lysates were directly used for in vitro phosphorylation using 2 μl AURKB lysate and 10 μl TERT lysate in phosphorylation buffer (10 mM HEPES [pH 7.4], 150 mM NaCl, 10 mM $MgCl_2$, and 1 mM EGTA) for 30 min at 37°C. The phosphorylation reaction was then diluted in TRAP lysis buffer (1:25) and used for a quantitative TRAP assay as described above.

ACCESSION NUMBERS

The RNA-seq and ChIP-seq data reported in this paper have been deposited in the Gene Expression Omnibus (GEO) under accession number GSE67133.

SUPPLEMENTAL INFORMATION

Supplemental Information includes six figures and one table and can be found with this article online at http://dx.doi.org/10.1016/j.celrep.2015.05.015.

AUTHOR CONTRIBUTIONS

J.-P.M. and K.R. designed the project, analyzed the data, and wrote the manuscript. J.-P.M. performed all experiments.

ACKNOWLEDGMENTS

We are grateful to Ulrike Müller and Frank Edenhofer for providing embryonic stems cells, Ute Schmidt for MS2 plasmids, and Sabrina Schumacher for excellent technical assistance. We thank Sarah Osterwald, Fabian Erdel, and Katharina Deeg for valuable comments on the manuscript. This work was supported by the German CellNetworks Cluster of Excellence (EXC81) and the project *CancerTelSys* (01ZX1302A) in the E:med program of the German Federal Ministry of Education and Research (BMBF).

Received: January 9, 2015
Revised: March 28, 2015
Accepted: May 11, 2015
Published: June 4, 2015

REFERENCES

Aagaard, L., Laible, G., Selenko, P., Schmid, M., Dorn, R., Schotta, G., Kuhfittig, S., Wolf, A., Lebersorger, A., Singh, P.B., et al. (1999). Functional mammalian homologues of the Drosophila PEV-modifier Su(var)3-9 encode

centromere-associated proteins which complex with the heterochromatin component M31. EMBO J. *18*, 1923–1938.

Adams, R.R., Carmena, M., and Earnshaw, W.C. (2001). Chromosomal passengers and the (aurora) ABCs of mitosis. Trends Cell Biol. *11*, 49–54.

Arnoult, N., Van Beneden, A., and Decottignies, A. (2012). Telomere length regulates TERRA levels through increased trimethylation of telomeric H3K9 and HP1α. Nat. Struct. Mol. Biol. *19*, 948–956.

Benetti, R., García-Cao, M., and Blasco, M.A. (2007a). Telomere length regulates the epigenetic status of mammalian telomeres and subtelomeres. Nat. Genet. *39*, 243–250.

Benetti, R., Gonzalo, S., Jaco, I., Schotta, G., Klatt, P., Jenuwein, T., and Blasco, M.A. (2007b). Suv4-20h deficiency results in telomere elongation and derepression of telomere recombination. J. Cell Biol. *178*, 925–936.

Blasco, M.A. (2007). The epigenetic regulation of mammalian telomeres. Nat. Rev. Genet. *8*, 299–309.

Bouzinba-Segard, H., Guais, A., and Francastel, C. (2006). Accumulation of small murine minor satellite transcripts leads to impaired centromeric architecture and function. Proc. Natl. Acad. Sci. USA *103*, 8709–8714.

Brown, K.E., Bagci, H., Soza-Ried, J., and Fisher, A.G. (2013). Atypical heterochromatin organization and replication are rapidly acquired by somatic cells following fusion-mediated reprogramming by mouse ESCs. Cell Cycle *12*, 3253–3261.

Cerone, M.A., Burgess, D.J., Naceur-Lombardelli, C., Lord, C.J., and Ashworth, A. (2011). High-throughput RNAi screening reveals novel regulators of telomerase. Cancer Res. *71*, 3328–3340.

Chung, I., Leonhardt, H., and Rippe, K. (2011). De novo assembly of a PML nuclear subcompartment occurs through multiple pathways and induces telomere elongation. J. Cell Sci. *124*, 3603–3618.

Ferri, F., Bouzinba-Segard, H., Velasco, G., Hubé, F., and Francastel, C. (2009). Non-coding murine centromeric transcripts associate with and potentiate Aurora B kinase. Nucleic Acids Res. *37*, 5071–5080.

Fischle, W., Wang, Y., Jacobs, S.A., Kim, Y., Allis, C.D., and Khorasanizadeh, S. (2003). Molecular basis for the discrimination of repressive methyl-lysine marks in histone H3 by Polycomb and HP1 chromodomains. Genes Dev. *17*, 1870–1881.

Fischle, W., Tseng, B.S., Dormann, H.L., Ueberheide, B.M., Garcia, B.A., Shabanowitz, J., Hunt, D.F., Funabiki, H., and Allis, C.D. (2005). Regulation of HP1-chromatin binding by histone H3 methylation and phosphorylation. Nature *438*, 1116–1122.

Fodor, B.D., Shukeir, N., Reuter, G., and Jenuwein, T. (2010). Mammalian Su(var) genes in chromatin control. Annu. Rev. Cell Dev. Biol. *26*, 471–501.

García-Cao, M., O'Sullivan, R., Peters, A.H., Jenuwein, T., and Blasco, M.A. (2004). Epigenetic regulation of telomere length in mammalian cells by the Suv39h1 and Suv39h2 histone methyltransferases. Nat. Genet. *36*, 94–99.

Grimm, D., Streetz, K.L., Jopling, C.L., Storm, T.A., Pandey, K., Davis, C.R., Marion, P., Salazar, F., and Kay, M.A. (2006). Fatality in mice due to oversaturation of cellular microRNA/short hairpin RNA pathways. Nature *441*, 537–541.

Guenatri, M., Bailly, D., Maison, C., and Almouzni, G. (2004). Mouse centric and pericentric satellite repeats form distinct functional heterochromatin. J. Cell Biol. *166*, 493–505.

Haendeler, J., Hoffmann, J., Rahman, S., Zeiher, A.M., and Dimmeler, S. (2003). Regulation of telomerase activity and anti-apoptotic function by protein-protein interaction and phosphorylation. FEBS Lett. *536*, 180–186.

Herbert, B.S., Hochreiter, A.E., Wright, W.E., and Shay, J.W. (2006). Nonradioactive detection of telomerase activity using the telomeric repeat amplification protocol. Nat. Protoc. *1*, 1583–1590.

Honda, R., Körner, R., and Nigg, E.A. (2003). Exploring the functional interactions between Aurora B, INCENP, and survivin in mitosis. Mol. Biol. Cell *14*, 3325–3341.

Ivaldi, M.S., Karam, C.S., and Corces, V.G. (2007). Phosphorylation of histone H3 at Ser10 facilitates RNA polymerase II release from promoter-proximal pausing in Drosophila. Genes Dev. *21*, 2818–2831.

Jacobs, S.A., and Khorasanizadeh, S. (2002). Structure of HP1 chromodomain bound to a lysine 9-methylated histone H3 tail. Science *295*, 2080–2083.

Jády, B.E., Richard, P., Bertrand, E., and Kiss, T. (2006). Cell cycle-dependent recruitment of telomerase RNA and Cajal bodies to human telomeres. Mol. Biol. Cell *17*, 944–954.

Jegou, T., Chung, I., Heuvelman, G., Wachsmuth, M., Görisch, S.M., Greulich-Bode, K.M., Boukamp, P., Lichter, P., and Rippe, K. (2009). Dynamics of telomeres and promyelocytic leukemia nuclear bodies in a telomerase-negative human cell line. Mol. Biol. Cell *20*, 2070–2082.

Kalitsis, P., Griffiths, B., and Choo, K.H. (2006). Mouse telocentric sequences reveal a high rate of homogenization and possible role in Robertsonian translocation. Proc. Natl. Acad. Sci. USA *103*, 8786–8791.

Kanellopoulou, C., Muljo, S.A., Kung, A.L., Ganesan, S., Drapkin, R., Jenuwein, T., Livingston, D.M., and Rajewsky, K. (2005). Dicer-deficient mouse embryonic stem cells are defective in differentiation and centromeric silencing. Genes Dev. *19*, 489–501.

Labrador, M., and Corces, V.G. (2003). Phosphorylation of histone H3 during transcriptional activation depends on promoter structure. Genes Dev. *17*, 43–48.

Lee, E.R., McCool, K.W., Murdoch, F.E., and Fritsch, M.K. (2006). Dynamic changes in histone H3 phosphoacetylation during early embryonic stem cell differentiation are directly mediated by mitogen- and stress-activated protein kinase 1 via activation of MAPK pathways. J. Biol. Chem. *281*, 21162–21172.

Lehnertz, B., Ueda, Y., Derijck, A.A., Braunschweig, U., Perez-Burgos, L., Kubicek, S., Chen, T., Li, E., Jenuwein, T., and Peters, A.H. (2003). Suv39h-mediated histone H3 lysine 9 methylation directs DNA methylation to major satellite repeats at pericentric heterochromatin. Curr. Biol. *13*, 1192–1200.

Li, H., Zhao, L.L., Funder, J.W., and Liu, J.P. (1997). Protein phosphatase 2A inhibits nuclear telomerase activity in human breast cancer cells. J. Biol. Chem. *272*, 16729–16732.

Liang, X.H., Vickers, T.A., Guo, S., and Crooke, S.T. (2011). Efficient and specific knockdown of small non-coding RNAs in mammalian cells and in mice. Nucleic Acids Res. *39*, e13.

Liokatis, S., Stützer, A., Elsässer, S.J., Theillet, F.X., Klingberg, R., van Rossum, B., Schwarzer, D., Allis, C.D., Fischle, W., and Selenko, P. (2012). Phosphorylation of histone H3 Ser10 establishes a hierarchy for subsequent intramolecular modification events. Nat. Struct. Mol. Biol. *19*, 819–823.

Lo, W.S., Trievel, R.C., Rojas, J.R., Duggan, L., Hsu, J.Y., Allis, C.D., Marmorstein, R., and Berger, S.L. (2000). Phosphorylation of serine 10 in histone H3 is functionally linked in vitro and in vivo to Gcn5-mediated acetylation at lysine 14. Mol. Cell *5*, 917–926.

Lowell, S., Benchoua, A., Heavey, B., and Smith, A.G. (2006). Notch promotes neural lineage entry by pluripotent embryonic stem cells. PLoS Biol. *4*, e121.

Mallm, J.P., Tschäpe, J.A., Hick, M., Filippov, M.A., and Müller, U.C. (2010). Generation of conditional null alleles for APP and APLP2. Genesis *48*, 200–206.

Martens, J.H., O'Sullivan, R.J., Braunschweig, U., Opravil, S., Radolf, M., Steinlein, P., and Jenuwein, T. (2005). The profile of repeat-associated histone lysine methylation states in the mouse epigenome. EMBO J. *24*, 800–812.

Mateescu, B., England, P., Halgand, F., Yaniv, M., and Muchardt, C. (2004). Tethering of HP1 proteins to chromatin is relieved by phosphoacetylation of histone H3. EMBO Rep. *5*, 490–496.

Müller-Ott, K., Erdel, F., Matveeva, A., Mallm, J.P., Rademacher, A., Hahn, M., Bauer, C., Zhang, Q., Kaltofen, S., Schotta, G., et al. (2014). Specificity, propagation, and memory of pericentric heterochromatin. Mol. Syst. Biol. *10*, 746.

Nowak, S.J., and Corces, V.G. (2004). Phosphorylation of histone H3: a balancing act between chromosome condensation and transcriptional activation. Trends Genet. *20*, 214–220.

Peters, A.H., O'Carroll, D., Scherthan, H., Mechtler, K., Sauer, S., Schöfer, C., Weipoltshammer, K., Pagani, M., Lachner, M., Kohlmaier, A., et al. (2001). Loss of the Suv39h histone methyltransferases impairs mammalian heterochromatin and genome stability. Cell *107*, 323–337.

Petti, E., Jordi, F., Buemi, V., Dinami, R., Benetti, R., Blasco, M.A., and Schoeftner, S. (2015). Altered telomere homeostasis and resistance to skin carcinogenesis in Suv39h1 transgenic mice. Cell Cycle *14*, 1438–1446.

Sasaki, N., Yamauchi, H., Tomohiro, N., and Agui, T. (2013). The telocentric tandem repeat at the p-arm is not conserved in Mus musculus subspecies. Gene *513*, 214–218.

Seimiya, H., Tanji, M., Oh-hara, T., Tomida, A., Naasani, I., and Tsuruo, T. (1999). Hypoxia up-regulates telomerase activity via mitogen-activated protein kinase signaling in human solid tumor cells. Biochem. Biophys. Res. Commun. *260*, 365–370.

Teif, V.B., Vainshtein, Y., Caudron-Herger, M., Mallm, J.P., Marth, C., Höfer, T., and Rippe, K. (2012). Genome-wide nucleosome positioning during embryonic stem cell development. Nat. Struct. Mol. Biol. *19*, 1185–1192.

Teperek-Tkacz, M., Meglicki, M., Pasternak, M., Kubiak, J.Z., and Borsuk, E. (2010). Phosphorylation of histone H3 serine 10 in early mouse embryos: active phosphorylation at late S phase and differential effects of ZM447439 on first two embryonic mitoses. Cell Cycle *9*, 4674–4687.

Tomlinson, R.L., Abreu, E.B., Ziegler, T., Ly, H., Counter, C.M., Terns, R.M., and Terns, M.P. (2008). Telomerase reverse transcriptase is required for the localization of telomerase RNA to cajal bodies and telomeres in human cancer cells. Mol. Biol. Cell *19*, 3793–3800.

Wenz, C., Enenkel, B., Amacker, M., Kelleher, C., Damm, K., and Lingner, J. (2001). Human telomerase contains two cooperating telomerase RNA molecules. EMBO J. *20*, 3526–3534.

Xi, P., Zhou, L., Wang, M., Liu, J.P., and Cong, Y.S. (2013). Serine/threonine-protein phosphatase 2A physically interacts with human telomerase reverse transcriptase hTERT and regulates its subcellular distribution. J. Cell. Biochem. *114*, 409–417.

Yamamoto, K., and Sonoda, M. (2003). Self-interaction of heterochromatin protein 1 is required for direct binding to histone methyltransferase, SUV39H1. Biochem. Biophys. Res. Commun. *301*, 287–292.

Zhao, Y.M., Li, J.Y., Lan, J.P., Lai, X.Y., Luo, Y., Sun, J., Yu, J., Zhu, Y.Y., Zeng, F.F., Zhou, Q., and Huang, H. (2008). Cell cycle dependent telomere regulation by telomerase in human bone marrow mesenchymal stem cells. Biochem. Biophys. Res. Commun. *369*, 1114–1119.

Cell Reports

Supplemental Information

Aurora Kinase B Regulates Telomerase Activity via a Centromeric RNA in Stem Cells

Jan-Philipp Mallm and Karsten Rippe

Supplemental Information

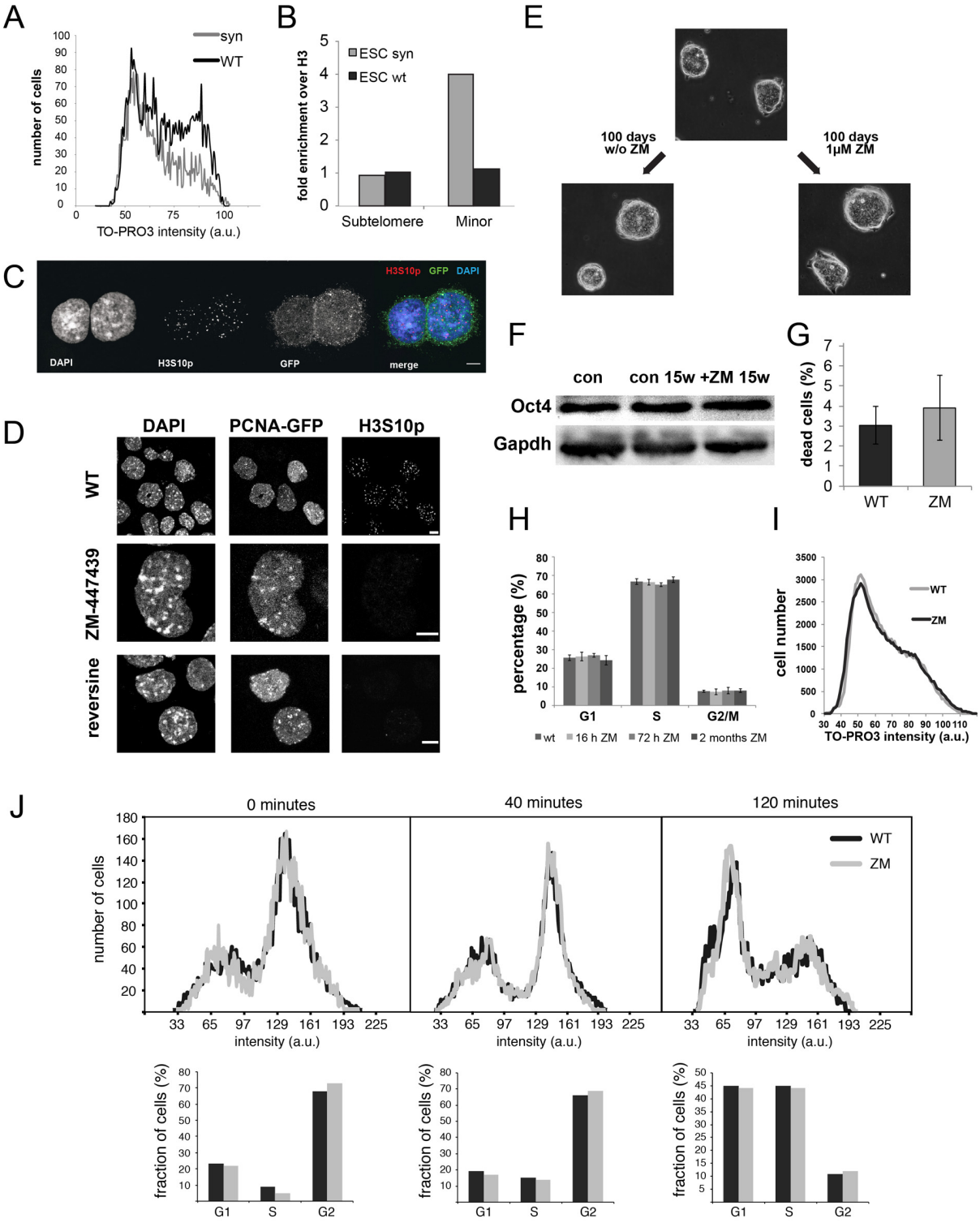

Figure S1, related to Figure 2. Enrichment of H3S10p at minor satellite and p-arm subtelomeres by AURKB.

(A) FACS cell cycle analysis of synchronized ESCs. ESCs synchronized with aphidicollin displayed a significant reduction of cells in G2/M (“syn”, grey line) as compared to untreated cells (“WT”, black line) but a residual fraction of G2/M cells remained.
(B) ChIP analysis of H3S10p enrichment. The enrichment of normalized mapped reads for ChIP-seq of H3S10p over H3 was calculated for minor satellite repeats and for the averaged subtelomeric regions located on chromosomal q-arms. The latter loci displayed no H3S10p foci in S-phase in the CLSM analysis since SPPs were found only on the p-arm. In the unsynchronized cells mitotic H3S10p covered the whole chromosome and dominates the signal with similar values for both subtelomeres and minor satellites. In the synchronized population with a reduced G2/M fraction, an enrichment of H3S10p in minor satellite repeats was apparent. This indicates that the H3S10p foci are found both at minor satellite repeats and between centromere and telomere as seen in the CLSM images. Data points are averages from two ChIP-seq reactions.
(C) Immunofluorescence of H3S10p in Oct4-GIP stem cells. SPPs were also present in ESCs that express GFP under the control of the *Pou5F1* promoter. Scale bar 5 µm.
(D) Loss of H3S10p induced by treating ESCs with the AURKB inhibitors ZM-447439 (1 µM) or reversine (0.5 µM). PCNA-GFP was used as a maker for S-phase.
(E) Bright-field images of ESC colonies. Morphology of ESCs did not change after long-term culturing for 100 days with ZM-447439 at a concentration of 1 µM. Thus, SPPs were lost during S-phase in the presence of inhibitor but cell division and the stem cell state were unperturbed.
(F) Western blot of OCT4 and GAPDH. Expression of OCT4 was unaffected by inhibition of AURKB.
(G) Fraction of dead cells measured with FACS by the uptake of TO-PRO3. Error bars represent the standard deviation of three independent replicates.
(H) Cell cycle progression in presence of 1 µM ZM-447439 measured by FACS analysis. Error bars were calculated from the standard deviation of three independent replicates.
(I) Representative FACS profile of untreated ESCs (WT) and ESCs treated for two months with ZM-447439 (ZM).
(J) ESCs arrested in mitosis with nocodazole and released for the time indicated. Cell cycle phases were determined from the cell cycle profiles.

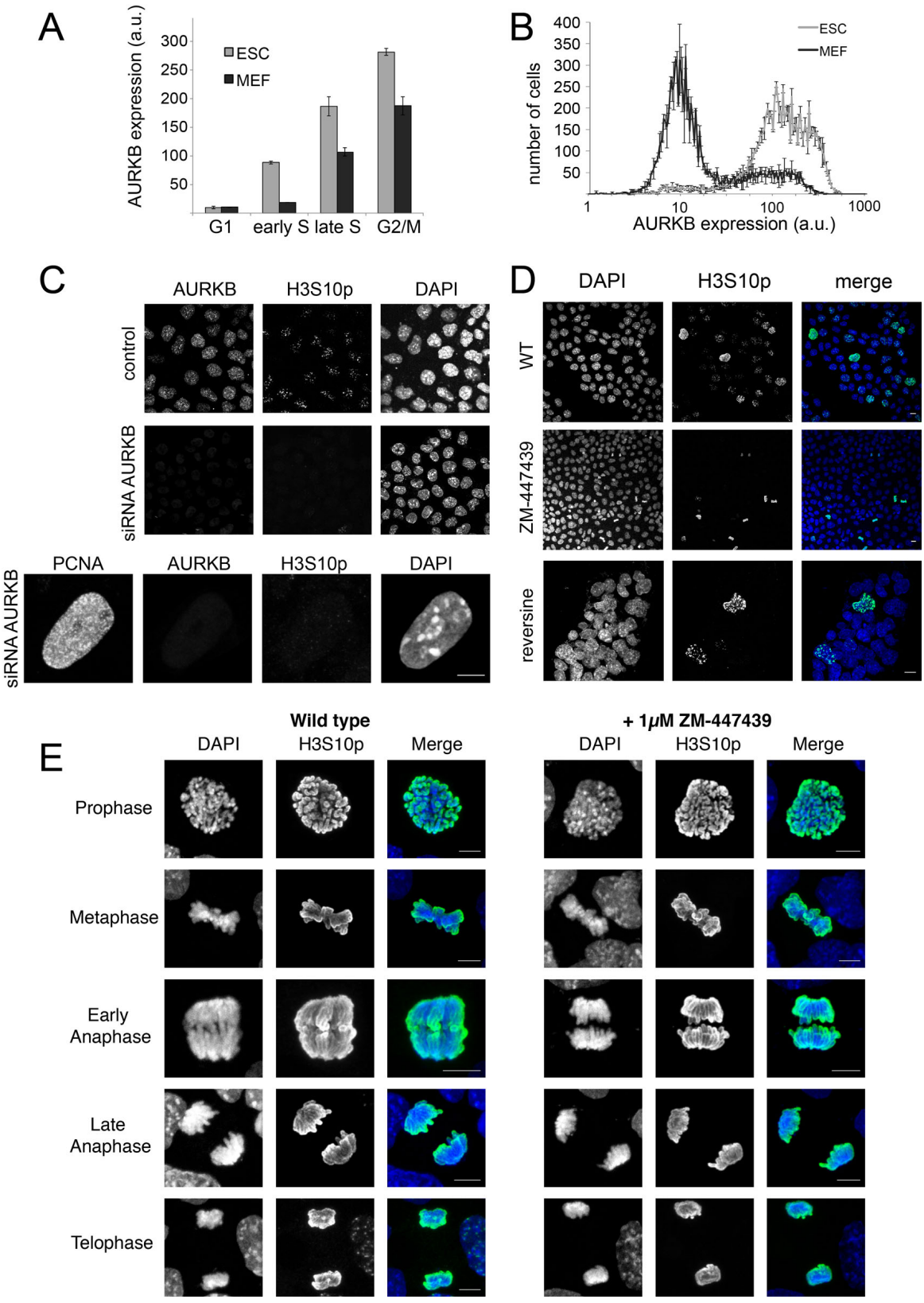

Figure S2, related to Figure 2. Expression of AURKB and CLSM images of H3S10p foci after AURKB inhibition/knockdown.

(A) Relative expression levels as measured by FACS for ESCs and MEFs. The cell cycles phases were determined from the DNA content. Error bars represent the standard deviation of three independent replicates.
(B) Relative expression levels of AURKB for the whole cell population of ESCs and MEFs. Error bars represent the standard deviation of three independent replicates.
(C) Knockdown of AURKB showing loss of H3S10p foci. Scale bar: 5 μm.
(D) Images of un-synchronized cells. It can be seen that at inhibitor concentrations of 1 μM ZM-447439 or 0.5 μM reversine H3S10p foci was lost during interphase but mitotic H3S10p was still present. In the merged image H3S10p is depicted in green, DAPI in blue. Scale bar: 10 μm.
(E) Representative images of mitotic ESCs untreated and treated with ZM-447439. In the merged image H3S10p is depicted in green, DAPI in blue. Scale bar: 5 μm.

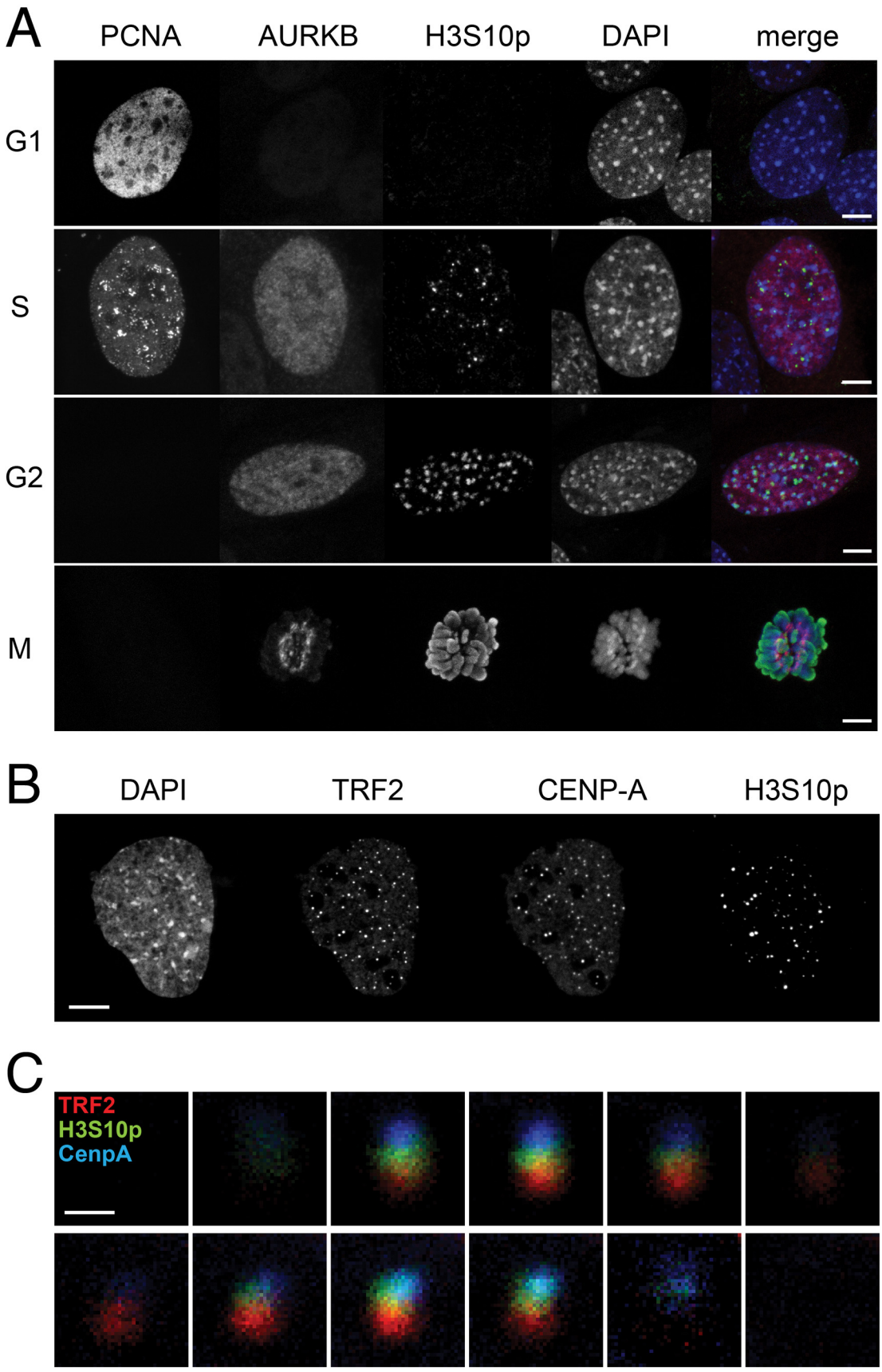

Figure S3, related to Figure 3. CLSM images of H3S10p foci in *Suv39h* dn iMEFs relative to centromeres and telomeres

(A) Cell-cycle dependent occurrence of H3S10p foci in *Suv39h* dn iMEFs. AURKB was expressed during S-phase and H3S10p foci were present. PCNA-GFP was used to distinguish between different cell-cycle stages. Scale bars: 5 μm.
(B) Localization of H3S10p foci relative to telomere and centromere in *Suv39h* dn iMEFs. Cells were transfected with RFP-TRF2 to detect the telomeres and immunostained for CENP-A and H3S10p. Scale bar: 5 μm.
(C) Enlarged view of two separate H3S10p loci with co-staining of telomere and centromere. The two rows of images taken along the optical axes from the CLSM 3D image stack show that the position of the H3S10p (green) was between the centromere (blue) and the telomere (red). In the top row all three signals were in the image plane, whereas in the bottom row the signals appeared sequentially. Scale bar: 0.5 μm.

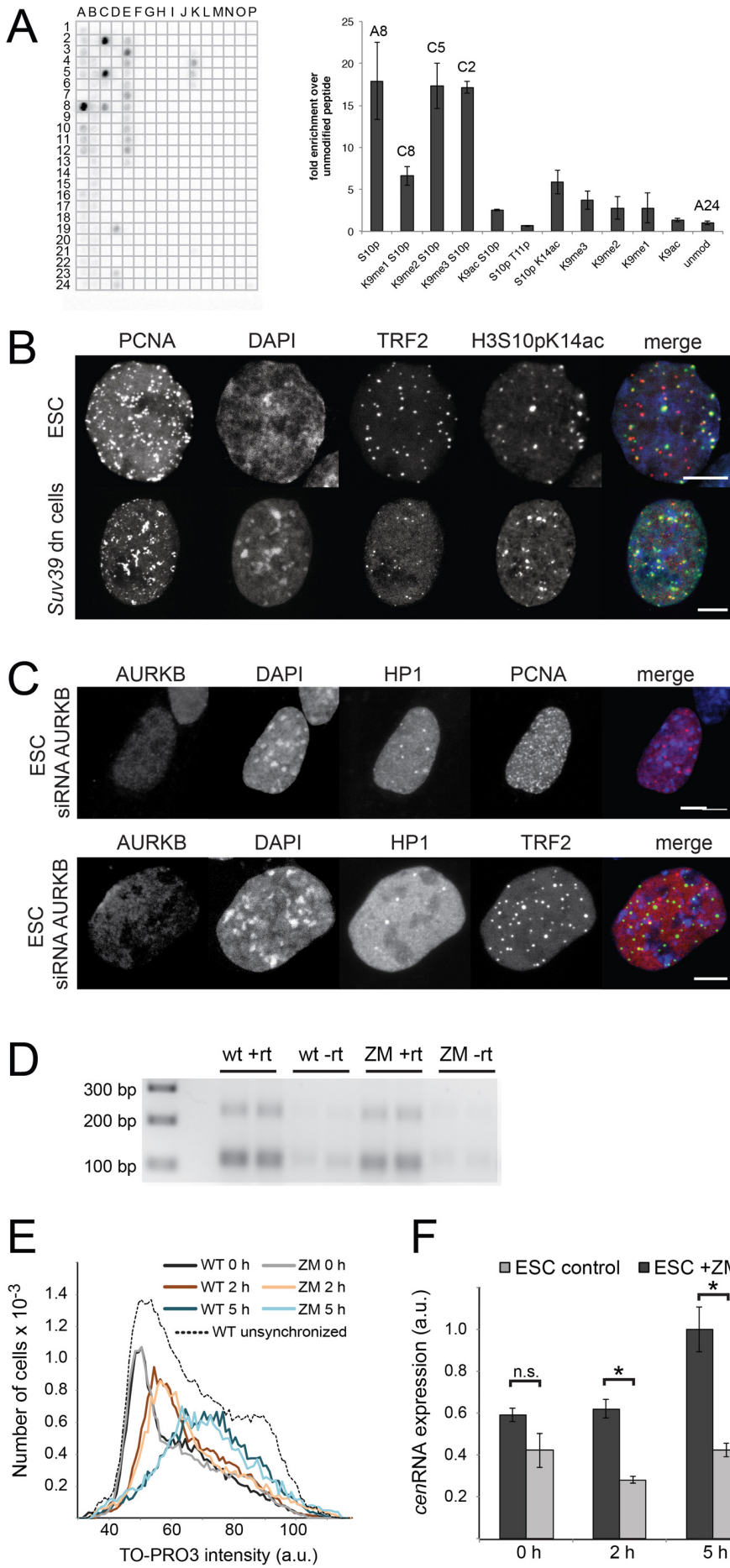
A
A B C D E F G H I J K L M N O P
1 2 3 4 5 6 7 8 9 10 11 12 13 14 15 16 17 18 19 20 21 22 23 24
fold enrichment over unmodified peptide
25 20 15 10 5 0
A8
C8
C5
C2
A24
S10p
K9me1 S10p
K9me2 S10p
K9me3 S10p
K9ac S10p
S10p T11p
S10p K14ac
K9me3
K9me2
K9me1
K9ac
unmod
B
PCNA
DAPI
TRF2
H3S10pK14ac
merge
ESC
Suv39 dn cells
C
AURKB
DAPI
HP1
PCNA
merge
ESC siRNA AURKB
AURKB
DAPI
HP1
TRF2
merge
ESC siRNA AURKB
D
wt +rt
wt -rt
ZM +rt
ZM -rt
300 bp
200 bp
100 bp
E
WT 0 h
ZM 0 h
WT 2 h
ZM 2 h
WT 5 h
ZM 5 h
WT unsynchronized
Number of cells x 10-3
1.4 1.2 1.0 0.8 0.6 0.4 0.2
40 60 80 100
TO-PRO3 intensity (a.u.)
F
ESC control
ESC +ZM
cenRNA expression (a.u.)
1.0 0.8 0.6 0.4 0.2
n.s.
*
*
0 h
2 h
5 h

Figure S4, related to Figure 3. Immunofluoresence of H3S10pK14ac and HP1 after AURKB knockdown; *cen*RNA expression after release into S-phase.

(A) Analysis of antibody for H3S10p on a peptide array of modified histone tails from Active Motif (#13001). On the left side the antibody blot is shown. The antibody used for detecting SPPs after overexpression of Suv39h1 was clearly specific for H3S10 phosphorylation despite the absence or presence of an adjacent lysine 9 methylation. Binding to relevant peptides was quantified for the indicated modifications and corresponding blot positions are indicated on the bar plots in the right figure panel. The complete annotation of the array is given at http://www.activemotif.com/documents/MODified_Histone_Peptide_Array_grid.xls. Error bars: Standard deviation of two experiments.

(B) Immunostaining of H3S10pK14ac in ESCs and *Suv39h* dn iMEFs. Cells were transfected with PCNA-GFP and RFP-TRF2. H3S10pK14ac was stained with an antibody detecting only the double modification, which was found close to telomeres in S-phase. In the merged image, TRF2 is shown in red, H3S10pK14ac in green and DAPI in blue. Scale bars: 5 μm.

(C) Immunostaining of HP1 after siRNA knockdown of AURKB. AURKB knockdown induced the formation of small dense HP1 foci that were located outside pericentric heterochromatin but close to telomeres. Scale bars: 5 μm.

(D) Agarose-gel to check absence of genomic DNA in RT-PCR *cen*RNA samples at the end-point of the PCR reaction. RNA was reverse transcribed in the presence or absence of ZM inhibitor. These samples were used as templates for RT-PCR. Samples without reverse transcriptase ("- rt") did not give raise to PCR products from centromeric repeats, as opposed to the samples that included reverse transcriptase ("+ rt") samples. Thus, genomic DNA contaminations were absent in the cDNA samples for *cen*RNA analysis. Quantification of *cen*RNA transcripts was done from Ct curves in the exponential amplification range.

(E) FACS cell cycle profile of synchronized cells. The "WT 0 h" profile corresponds to cells arrested for 20 hours with aphidicolin. The "WT 2 h" and "WT 5 h" samples were released for two or five hours respectively. The ZM samples were synchronized accordingly but in presence of the AURKB inhibitor ZM-447439 at 1 μM concentration. The dashed line shows the profile of unsynchronized cells.

(F) Expression level of *cen*RNA after G1/S release measured by RT-PCR. Expression level of *cen*RNA was highest in control cells released for five hours. The expression level in inhibitor treated cells did not change upon release from the cell cycle arrest and progression into S-phase was not impaired (see panel A). Error bars represent the standard deviation of three independent samples.

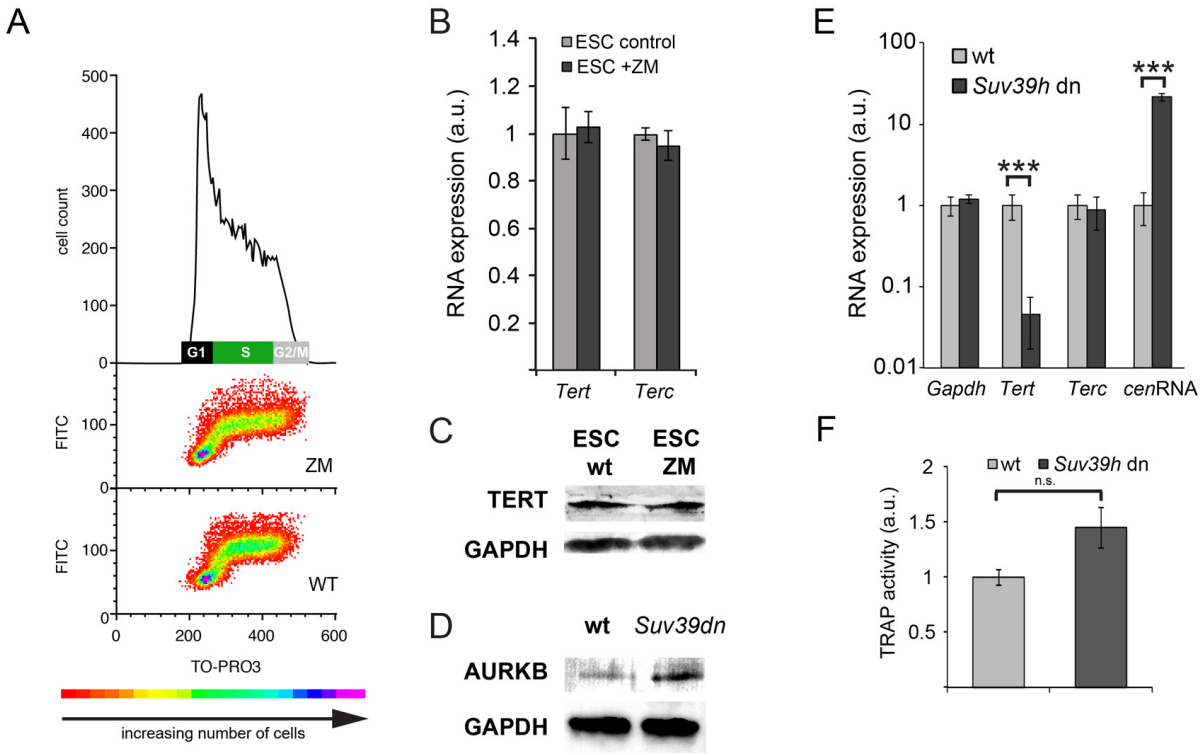

Figure S5, related to Figure 4. Replication timing after AURKB inhibition and expression of TERT and TERC in ESCs and *Suv39h* dn iMEFs

(A) Plot of telomere probe intensity (FITC) and DNA content (TO-PRO3). A doubling of the telomere signal at the onset of S-phase was observed in both wild type and ZM-447439 treated cells. The color code represents the number of cells with the given intensities.

(B) *Tert* and *Terc* RNA expression levels in ESCs determined by RT-PCR in dependence of AURKB inhibition. Values were normalized using β-actin. RNA expression of both the protein and RNA component of telomerase remained unchanged. Error bars correspond to the standard deviation of three independent replicates.

(C) Western blot of TERT and GAPDH. After AURKB inhibition TERT protein levels remained unchanged.

(D) Western blot of AUKRB and GAPDH. AURKB expression was higher in *Suv39* dn cells as compared to wild type iMEFs.

(E) RNA expression level of *Tert*, *Terc* and *cen*RNAs in *Suv39h* dn iMEFs measured by RT-PCR. A 22-fold higher expression of *cen*RNA and a reduced *Tert* expression was observed in *Suv39h* dn iMEFs as compared to wild type cells. Values were normalized to β-actin expression. Note that the y-axis is plotted with a log scale. Error bars correspond to the standard deviation of three independent replicates.

(F) Quantitative TRAP assay of telomerase activity. Telomerase activity in *Suv39h* dn iMEFs was slightly higher despite the lower *Tert* expression (*p*-value 0.08). Thus, overexpression of *cen*RNA compensated for lower *Tert* expression in *Suv39h* dn iMEFs. Error bars correspond to the standard deviation of three independent replicates.

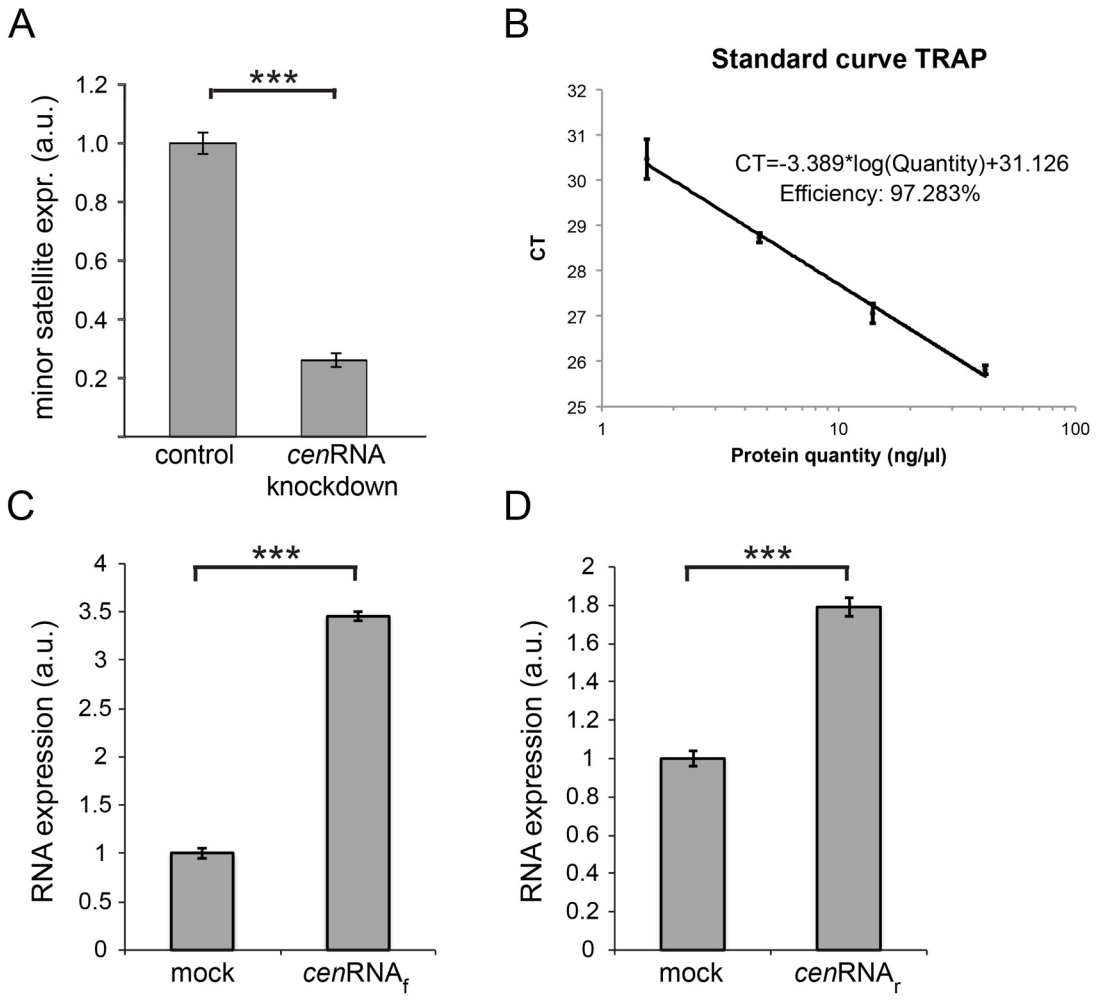

Figure S6, related to Figure 4. Knockdown *cen*RNA and overexpression

(A) Efficiency of *cen*RNA knockdown. Transfection of cells with *cen*RNA antisense oligonucleotides reduced the amount of *cen*RNA from both strands by 74%. Error bars correspond to the standard deviation of three independent replicates.

(B) Standard curve for quantification of telomerase activity by RT-PCR. Four different dilutions of cell lysate were used in the TRAP assay. The regression line was calculated from three individual measurements per dilution and the standard deviation per dilution is represented by the error bars.

(C) Quantification of *cen*RNA$_f$ overexpression by RT-PCR. The *cen*RNA$_f$ sequence was overexpressed three fold from a construct with an U6 RNA polymerase III promoter. Error bars represent the standard deviation of three independent experiments.

(D) Same as panel C but for *cen*RNA$_r$. Over-expression of this RNA was about two fold. Error bars represent the standard deviation of three independent experiments.

Supplemental Tables

Gene Id	Symbol	log2-fold change of transcripts	p-value
19659	Rbp1	4.7	4.37E-03
271844	Pla2g4f	3.7	3.79E-03
69219	Ddah1	2.0	2.75E-08
235505	Cd109	1.6	5.38E-03
228432	Ano3	1.3	2.50E-03
235281	Scn3b	1.3	4.27E-03
12519	Cd80	1.3	9.46E-03
213783	Plekhg1	1.1	1.11E-03
19250	Ptpn14	1.1	3.42E-05
20720	Serpine2	1.0	1.01E-03

Table S1, related to Figure 4. Differential expression analysis of ZM-447439-treated cells compared to wild type ESCs.

Ten genes were identified using DESeq with two replicates for treated and untreated cells each that were significantly upregulated. No gene was found to be down-regulated by at least 2-fold.